NASA Technical Memorandum 106067

Fiber Shape Effects on Metal Matrix Composite Behavior

H.C. Brown
Sverdrup Technology, Inc.
Lewis Research Center Group
Brook Park, Ohio

H.-J. Lee and C.C. Chamis
National Aeronautics and Space Administration
Lewis Research Center
Cleveland, Ohio

Prepared for the
37th International SAMPE Symposium and Exhibition
sponsored by the Society for the Advancement of Materials
and Process Engineering
Anaheim, California, March 9–12, 1992

NASA

FIBER SHAPE EFFECTS ON METAL MATRIX COMPOSITE BEHAVIOR

H.C. Brown
Sverdrup Technology, Inc.
Lewis Research Center Group
Brook Park, Ohio 44142

and

H.-J. Lee and C.C. Chamis
National Aeronautics and Space Administration
Lewis Research Center
Cleveland, Ohio 44135

SUMMARY

The effects of different fiber shapes on the behavior of a SiC/Ti-15 metal matrix composite is computationally simulated. A three-dimensional finite element model consisting of a group of nine unidirectional fibers is used in the analysis. The model is employed to represent five different fiber shapes: a circle, an ellipse, a kidney, and two different cross shapes. The distribution of microstresses and the composite material properties, such as moduli, coefficients of thermal expansion, and Poisson's ratios, are obtained from the finite element analysis for the various fiber shapes. Comparisons of these results are used to determine the sensitivity of the composite behavior to the different fiber shapes and assess their potential benefits. No clear benefits result from different fiber shapes though there are some increases/decreases in isolated properties.

BACKGROUND

Metal matrix composites offer great potential for use in advanced aerospace structural applications requiring high operational temperatures. These materials exhibit high stiffness to weight ratios at the anticipated use temperatures (between 425 and 1315 °C) and are currently

under development for use in compressor and turbine disks, blades and vanes. However, before metal matrix composites can be used in these critical applications, key issues involving coefficient of thermal expansion mismatch, interface characterization, ductility and durability of the matrix, and identification of failure mechanisms must be resolved. A possible method for improving composite properties, especially in the transverse direction, may be to use noncirculat fiber shapes.

Ongoing research at NASA Lewis Research Center has been focused on computationally simulating the behavior of metal matrix composites. The computational methodologies have been based on simplified micromechanics equations and three-dimensional finite element analysis. These methods are not intended to replace experimental work, but to be used concurrently in the characterization of metal matrix composite behavior. The inherent advantage in computational methods lies in the tremendous savings in time and cost over experimental procedures. Ideally, computational methods can be used to perform an assessment of metal matrix composite behavior in order to focus experimental efforts into specific areas.

The purpose of this study is to assess the potential benefits to be gained from using non-circular fiber shapes. A three-dimensional finite element analysis is performed to computationally simulate the effect of five different fiber shapes on the composite behavior of a SiC/Ti-15 metal matrix composite. Results from the finite element analysis include both composite material properties and microstress distributions and are used to assess the effect of the various fiber shapes.

COMPUTATIONAL SIMULATION PROCEDURE

A linear elastic simulation is conducted using Version 65 of MSC/NASTRAN (1), a general purpose finite element package. The finite element model used in the study is a modified version of a unit cell originally developed by Caruso (2). The model consists of a group of nine unidirectional fibers in a three by three unit cell array as shown in figures 1 and 2. The finite element mesh consists of 8 bays along the length of the fiber where each cell consists of 64 six-sided solid elements (CHEXA) and 16 five-sided solid elements (CPENTA) for a total of 5760 elements and 5992 nodes. Extensive previous efforts using this model include exploring the effects of partial bonding and fiber fracture (3), predicting ply properties of metal matrix composites (4), and simulating compliant layers (5). More recent work has been related to modelling both fiber pushout (6) and microfracture in metal matrix composites (7-10).

The unit cell is modelled to allow the fiber volume ratio (FVR) to be easily varied. This is accomplished by assigning fiber material properties to the desired elements starting from the center of the unit cell. The remaining elements are then designated with matrix material properties. An interphase can also be easily modelled by assigning appropriate properties to elements between the fiber and the matrix. However, for the purposes of this study a perfect bond between the fiber and matrix is assumed. As mentioned before, five different fiber shapes are modelled: (1) a circle, (2) an ellipse, (3) a kidney shape, (4) a short cross shape, and (5) a long cross shape. The representations of the different shapes using the unit cell model are shown in figure 3. Each fiber shape is examined for three different FVR's. Due to the arrangement of elements in the unit cell, each fiber shape has a particular set of FVR's associated with it as listed in Table I.

A silicon carbide (SiC) fiber reinforced titanium (Ti-15-3) metal matrix composite is chosen for this study. This material represents one of the promising candidates for high temperature engine applications (11). Constituent properties for the fiber and matrix were obtained from Lerch (12) and are listed in Table II.

For each fiber shape three normal composite moduli (E_{11}, E_{22}, E_{33}), three shear composite moduli (G_{21}, G_{31}, G_{23}), three Poisson's ratios (ν_{12},ν_{13},ν_{23}), three coefficients of thermal expansion (α_{11}, α_{22}, α_{33}), and axial, radial, and hoop microstresses in the fiber and matrix are determined from the analysis. A total of seven separate MSC/NASTRAN simulations are required to predict the various composite properties and microstresses for each FVR of a given fiber shape. In a typical simulation, the various loadings and boundary conditions are applied through enforced displacements (13). To determine the normal moduli and Poisson's ratios, tensile loads are applied. For example, E_{11}, ν_{12}, and ν_{13} are determined by constraining the back face of the model and displacing the front face 0.003 cm in the x direction. A similar method is used to find the transverse moduli and the remaining Poisson's ratios. The shear moduli are found through shear loadings and thermal loads are applied to determine the coefficients of thermal expansion. Microstresses are calculated for each loading condition.

RESULTS AND DISCUSSION

For the purpose of convenient comparisons in the following sections, the results obtained for the circular fiber shape are used as a reference case against which results from the other four fiber shapes are compared. Due to the large amount of data obtained from the analysis, only the significant results will be discussed in detail in the subsequent sections. The selected results are chosen to bring to light the key aspects of fiber shape effects on the composite behavior.

However, for completeness all results from the analysis not shown in the text are included in Appendix A (for composite properties) and Appendix B (for microstresses).

Fiber Shape Effects on Composite Properties:

The effect of the different fiber shapes on longitudinal modulus, E_{11}, is illustrated in figure 4. Results for all five fiber shapes fall on the same line, indicating that longitudinal modulus is insensitive to the shape of the fiber. This is expected since E_{11} is mostly a fiber dominated property which depends on the amount of fiber, not the shape.

This behavior is not true, however, for the transverse case. In figure 5, the in-plane transverse modulus (E_{22}) of all the fiber shapes shows an increase from the circular shape modulus. The increase in transverse modulus results from the presence of more fiber in the 22-direction for the non-circular fiber shapes (see figure 3). Thus, the kidney and long cross shapes, which contain the largest amount of fiber in the 22-direction of all five shapes, show the greatest increase (about 6%) in transverse modulus.

Results for the G_{31} shear modulus are shown in figure 6. For this case, the response of the fiber shapes can be divided into two groups. The first group consists of the two cross shapes, which contain more fiber in the 33-direction than the circular shape, and shows an increase (9% for the long cross) in shear modulus. The second set, called the oblong group, is composed of the elliptic and kidney shapes, contains less fiber in the 33-direction, and shows a decrease (3% for both shapes) in shear modulus. These predictions are consistent with the expected behavior in which the amount of fiber dictates the stiffness of the shear modulus.

A look at Poisson's ratio, ν_{13}, in figure 7 shows that it is also influenced by fiber geometry. Similar to the shear modulus, the fiber shape responses fall on either side of the baseline response. The presence of more fiber in the 33-direction for the cross shape group results in a decrease in value (2% for the long cross). On the other hand, the oblong group shows a corresponding increase (2% for the kidney shape) due to the presence of less fiber in the 33-direction.

The influence of fiber shape on the coefficients of thermal expansion (CTE) follows the same trends as noted above. Fiber geometry has no effect on the longitudinal CTE as shown in figure 8. As mentioned before, longitudinal properties are dominated by the amount, not shape, of the fiber. The behavior of CTE through the thickness (33-direction) is again characterized by the two groups (figure 9). The oblong shapes have a higher CTE by approximately 3%. The cross shapes have a lower CTE by approximately 2%. The relative quantity of fiber in the 33-direction determines whether the composite CTE will be increased or decreased.

The influence of fiber shapes on composite material properties is summarized in Table III. This table shows whether a particular property for a particular shape increases, decreases, or remains the same when compared to the circular shape behavior. Although this table does not represent magnitude, it does highlight the pattern of the changes. In general, the longitudinal (fiber dominated) properties show no change. The transverse and shear moduli increase while CTE's and Poisson's ratios decrease.

Fiber Shape Effects on Microstresses:

The effect of fiber shapes on the distribution of microstresses in the composite is determined by examining the microstresses at four points in the center cell of the three by three unit cell array. The four points are indicated in figure 10 for each fiber shape: point A in the fiber, point B on the fiber side of the fiber-matrix boundary, point C on the matrix side of the boundary, and point D in the matrix. The microstresses are examined for one value of fiber volume ratio for each fiber shape, since similar trends occur for the other fiber volume ratios.

The results for axial microstresses under a longitudinal load are shown in figure 11. The majority of the stress is carried uniformly by the fiber while the matrix bears about one-fourth of the fiber load. Microstresses in both the fiber and matrix remain the same for all five shapes, indicating that fiber shapes have no effect axially under a longitudinal load. Once again, this results from the dominance of the fiber properties in the longitudinal direction, which is determined by the amount, not shape, of the fiber.

The radial microstresses under a transverse load are shown in figure 12. The circular fiber shape results in the lowest and most consistent values of microstresses at the four evaluation points. The elliptic and kidney shapes also have fairly consistent microstress values, but result in roughly a 10-15% increase in microstress over the circular shape. The long and short cross shapes both lead to the formation of large stress concentrations on the fiber side of the fiber-matrix boundary (point B). The result for both cross shapes is a 50% increase in microstress from the circular shape at point B. The large peaks in microstress for the cross shapes arise due to the presence of sharp projections in their fiber geometry. The circle, ellipse, and kidney shapes have a smoother geometry which results in a more consistent microstress distribution.

Even under a thermal load ($\Delta T = 38°$ C), the axial microstresses for the two cross shapes experience abrupt jumps as shown in figure 13. The microstresses for the circle and oblong shapes are reasonably close. The microstresses at point B for the short crosses increases by 29%, while the long cross jumps by 46% over the circular shape. Again, these microstress concentrations are due to the sharp geometry of the cross shapes.

CONCLUSIONS

Three clear points can be obtained from the results. First, the shape of the fiber does not influence the longitudinal properties since they are a function of the quantity, not geometry, of the fiber. Second, the transverse and shear material properties are only moderately affected by fiber shape. In most instances, the difference between the circular fiber and another shape is less than 10%. The most consistent improvements in composite properties occurred for the long cross fiber shape. Third, the effects of these improvements were dramatic increases in stress concentrations for the cross shapes and generally increased microstress values for the oblong shapes. Thus, results of this study indicate that the use of different fiber shapes is appropriate for applications in which the advantages of improving the transverse composite properties outweigh the trade-off of increased microstresses.

REFERENCES

1. MSC/NASTRAN, Version 65, Vol. I and II, User's Manual. The MacNeal-Schwendler Corporation, Los Angeles, CA.

2. Caruso, J.J., "Application of Finite Element Substructuring to Composite Micromechanics," NASA TM-83729, 1984.

3. Caruso, J.J., Trowbridge, D., and Chamis C.C., "Finite Element Applications to Explore the Effects of Partial Bonding on Metal Matrix Composite Properties," NASA TM-101482, 1989.

4. Caruso, J.J. and Chamis, C.C., "Prediction of High Temperature Metal Matrix Composite Ply Properties," NASA TM-102490, 1988.

5. Caruso, J.J., Chamis, C.C., and Brown, H.C., "Parametric Studies to Determine the Effect of Compliant Layers on Metal Matrix Composite Systems," NASA TM-102465, 1990.

6. Mital, S.K. and Chamis, C.C., "Fiber Pushout Test: A Three-Dimensional Finite Element Computational Simulation," NASA TM-102565, 1990.

7. Mital, S.K., Caruso, J.J., and Chamis, C.C., "Metal Matrix Composites Microfracture: Computational Simulation," NASA TM-103153, 1990.

8. Mital, S.K. and Chamis, C.C., "Microfracture in High Temperature Metal Matrix Crossply Laminates," NASA TM-104381, 1991.

9. Mital, S.K., Chamis, C.C., and Gotsis, P.K., "Microfracture in High Temperature Metal Matrix Laminates," NASA TM-105189, 1991.

10. Mital, S.K. and Chamis, C.C., "Thermally-Driven Microfracture in High Temperature Metal Matrix Composites," NASA TM-105305, 1991.

11. Lerch, B.A. and Saltsman, J.F., "Tensile Deformation Damage in SiC Reinforced Ti-15V-3Cr-3Al-3Sn," NASA TM-103620, 1991.

12. Lerch, B.A.: Private communication, NASA Lewis Research Center, November 1989.

13. Trowbridge, D., "Superelement Methods in High Temperature Metal Matrix Composites," Master's Thesis, Department of Civil Engineering, University of Akron, May 1989.

TABLE I.—FIBER SHAPE WITH CORRESPONDING FIBER VOLUME RATIOS

Fiber shape	Fiber volume ratios
Circle	0.136, 0.224, 0.334
Ellipse	0.103, 0.180, 0.279
Kidney	0.163, 0.257, 0.373
Long cross	0.147, 0.235, 0.345
Short cross	0.103, 0.180, 0.279

TABLE II.—ROOM TEMPERATURE CONSTITUENT MATERIAL PROPERTIES

	SiC	Ti-15
Young's modulus, E, GPa	427.5	84.8
Poisson's ratio, ν	0.190	0.320
Coefficients of thermal expansion, α, $\frac{ppm}{^\circ C}$	4.896	8.460
Density, ρ, kg/m^3	1.760	2.752

TABLE III.—TRENDS IN COMPOSITE PROPERTIES OF FIBER SHAPES IN COMPARISON WITH THE CIRCULAR SHAPE

Fiber shape	Composite modulus			Shear modulus			Coefficient of thermal expansion			Poisson's ratio		
	E_{11}	E_{22}	E_{33}	G_{21}	G_{31}	G_{23}	α_{11}	α_{22}	α_{33}	ν_{12}	ν_{13}	ν_{23}
	Equality (E) with or decrease (D) or increase (I) from circular shape value of above property											
Ellipse	E	I	E	I	D	I	E	D	I	D	I	D
Kidney	E	I	E	I	D	I	E	D	I	D	I	D
Long cross	E	I	I	I	I	I	E	D	D	D	D	D
Short cross	E	I	I	I	I	I	E	D	D	D	D	D

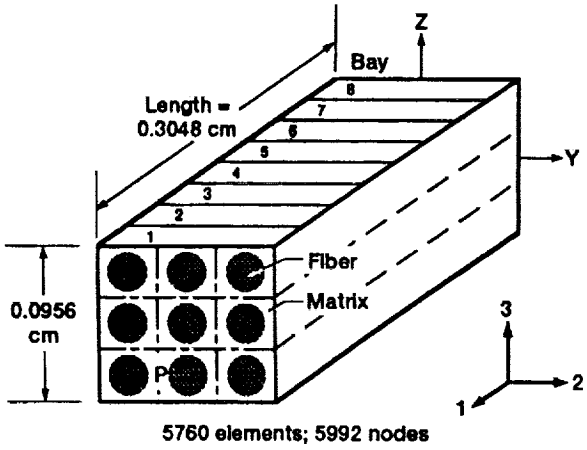

Figure 1.—Representation of nine-cell model finite element mesh.

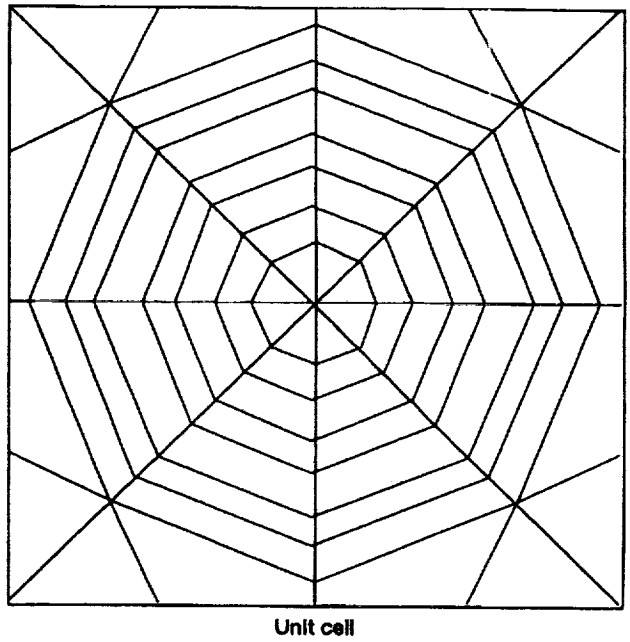

Figure 2.—Representation of a unit cell of the nine-cell model finite element mesh.

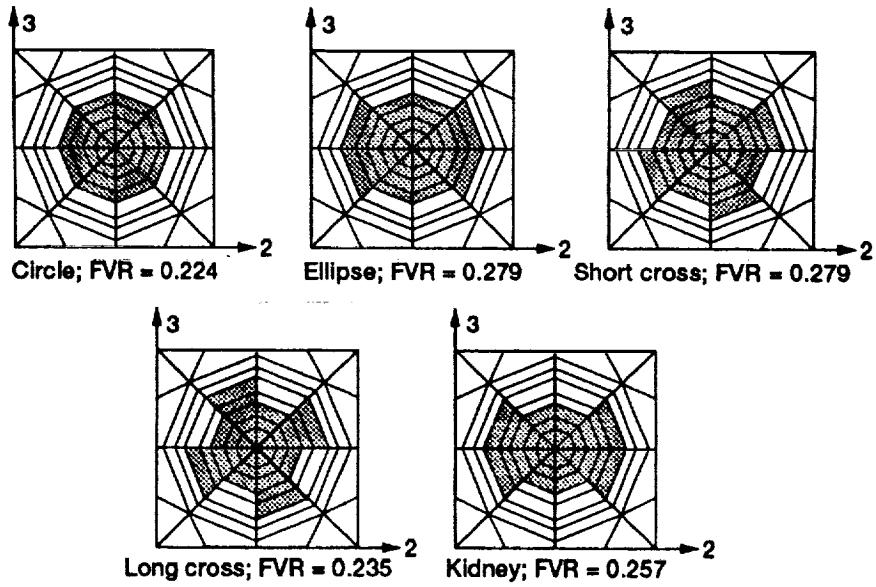

Figure 3.—Fiber shapes investigated.

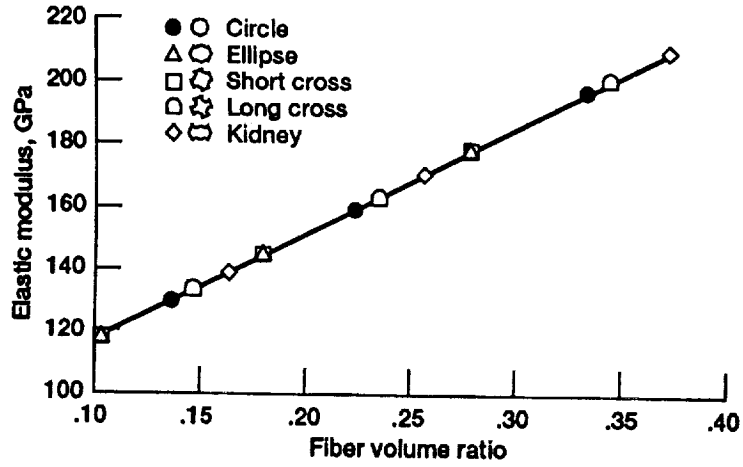

Figure 4.—Influence of fiber shape on longitudinal modulus (E_{11}) of SiC/Ti-15-3.

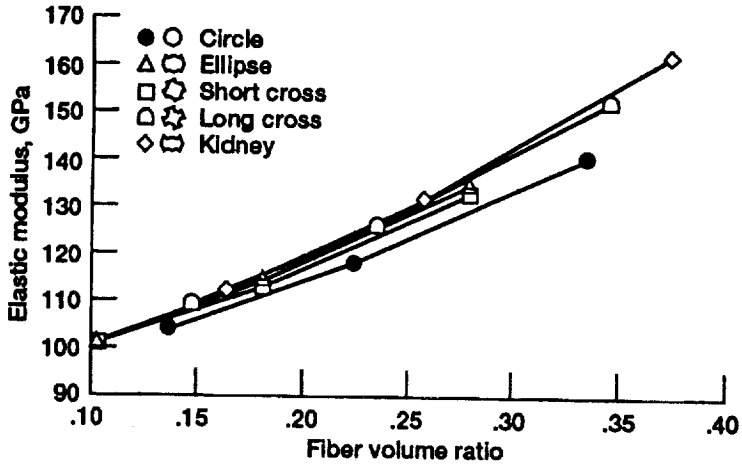

Figure 5.—Influence of fiber shape on transverse modulus (E_{22}) of SiC/Ti-15-3.

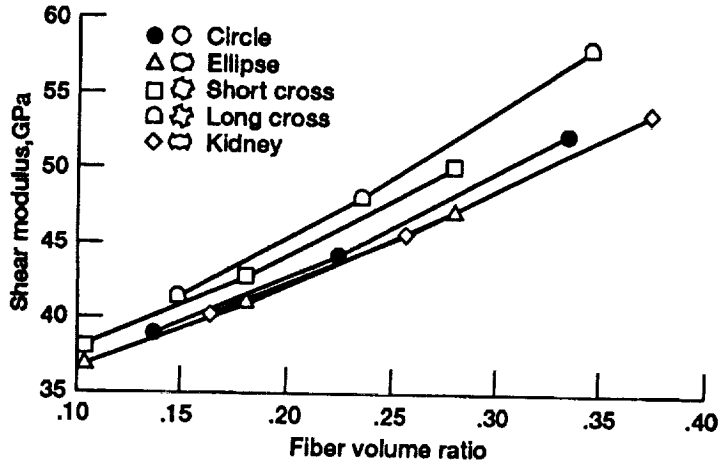

Figure 6.—Influence of fiber shape on shear modulus (G_{31}) of SiC/Ti-15-3.

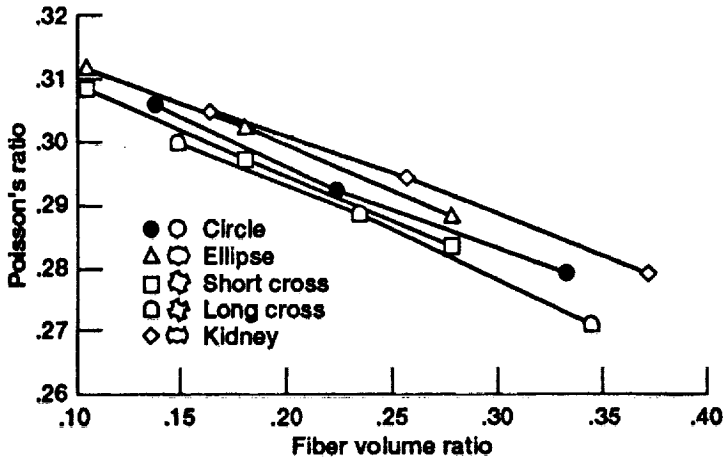

Figure 7.—Influence of fiber shape on Poisson's ratio (ν_{13}) of SiC/Ti-15-3.

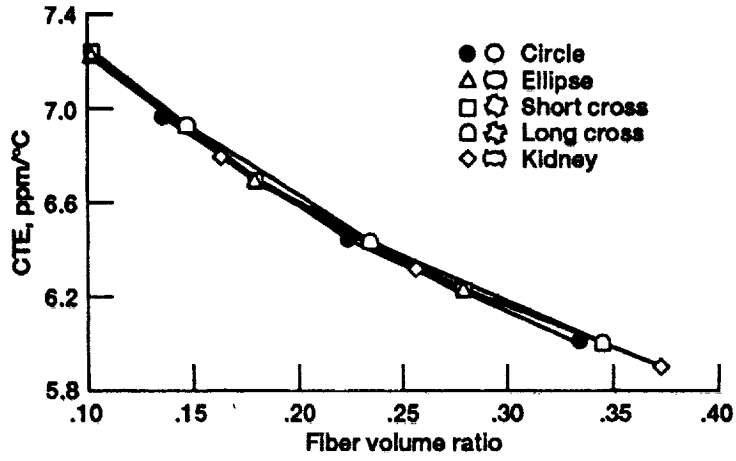

Figure 8.—Influence of fiber shape on longitudinal coefficient of thermal expansion (α_{11}) of SiC/Ti-15-3.

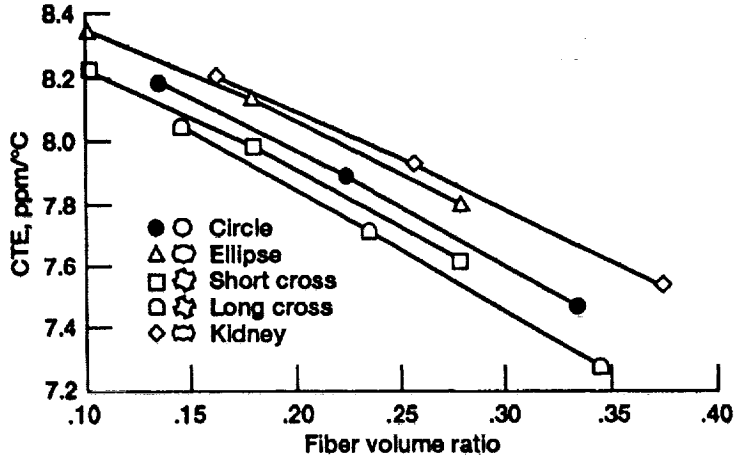

Figure 9.—Influence of fiber shape on transverse coefficient of thermal expansion (α_{33}) of SiC/Ti-15-3.

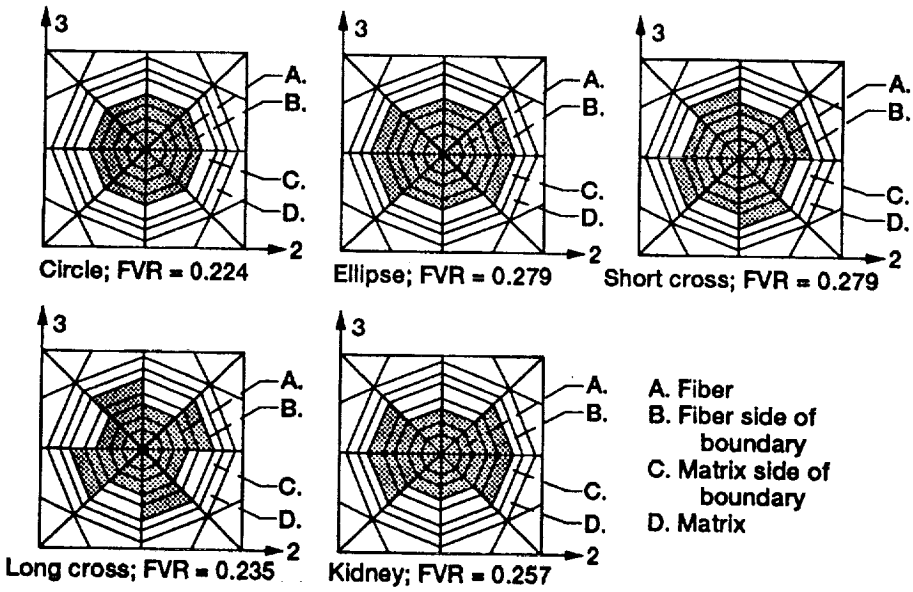

Figure 10.—Fiber shapes investigated.

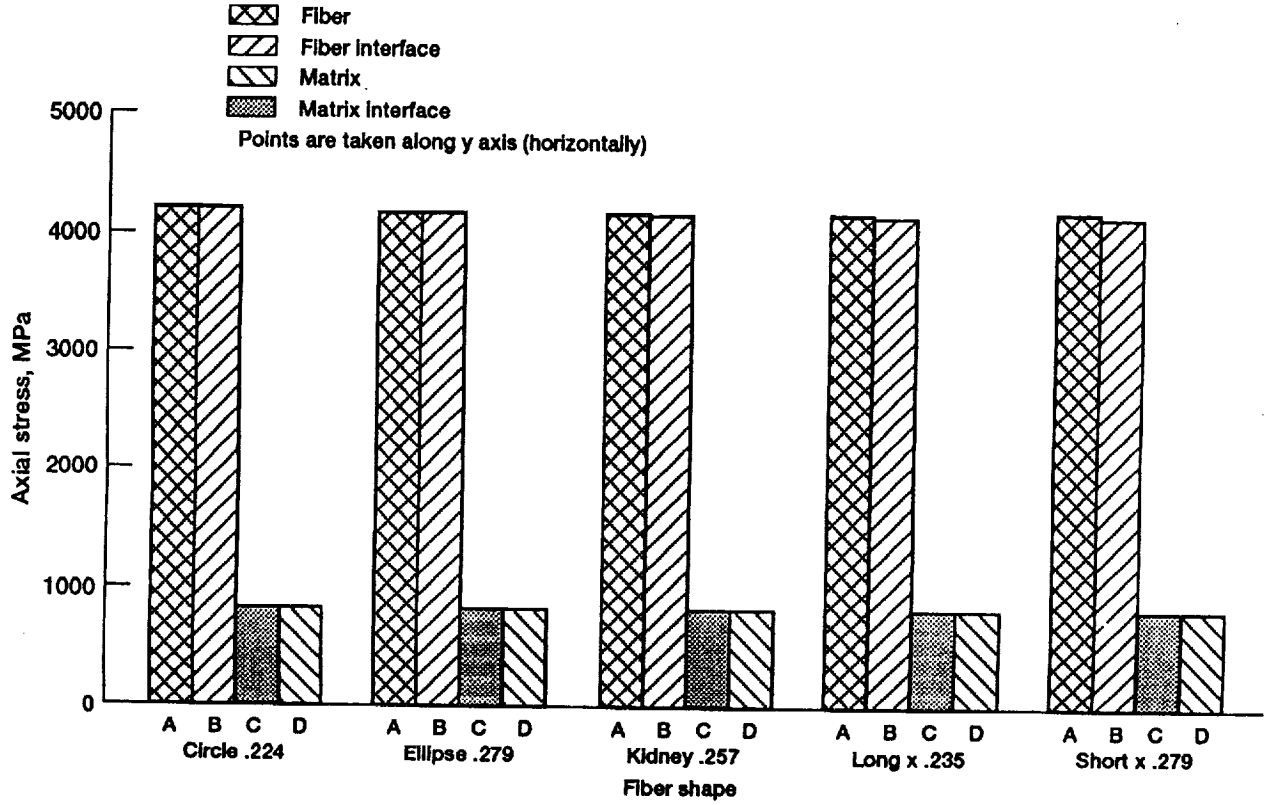

Figure 11.—Effect of fiber shape on axial stresses under a longitudinal load.

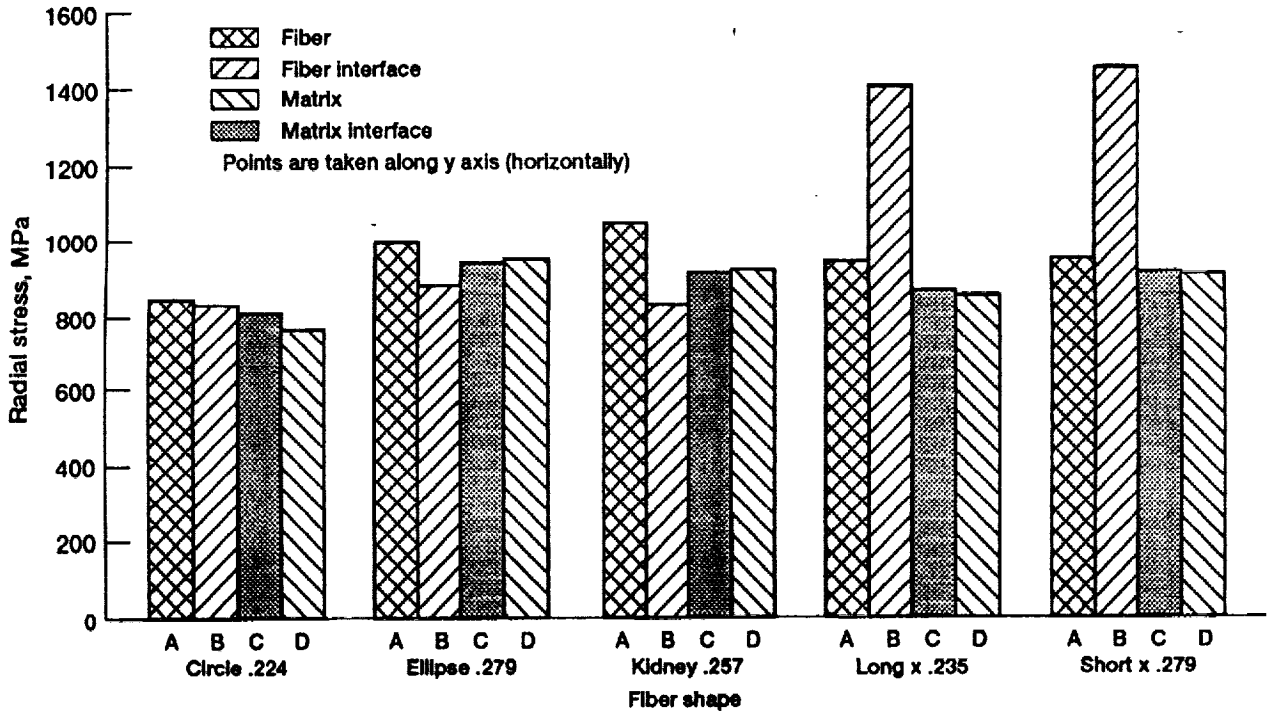

Figure 12.—Effect of fiber shape on radial stresses under a transverse load.

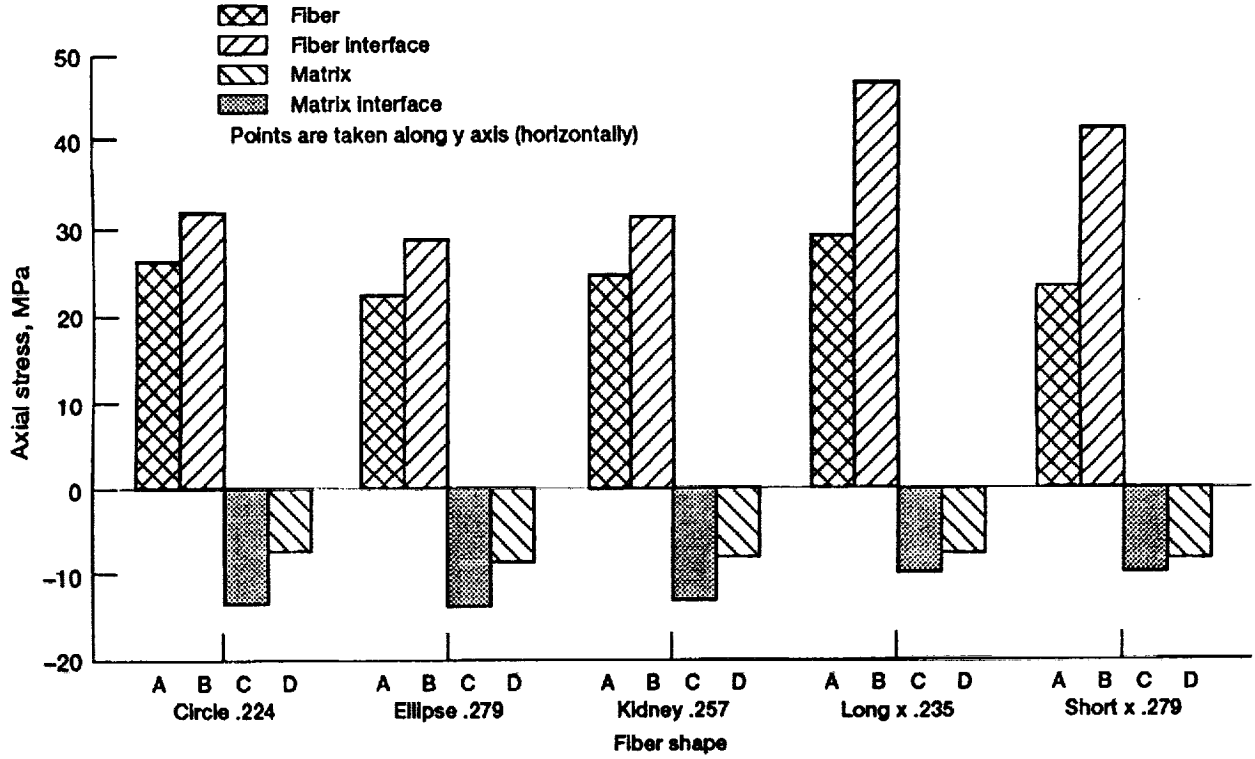

Figure 13.—Effect of fiber shape on axial stresses under a thermal load, (ΔT = 38 °C).

Appendix A:

Additional Composite Material Property Figures

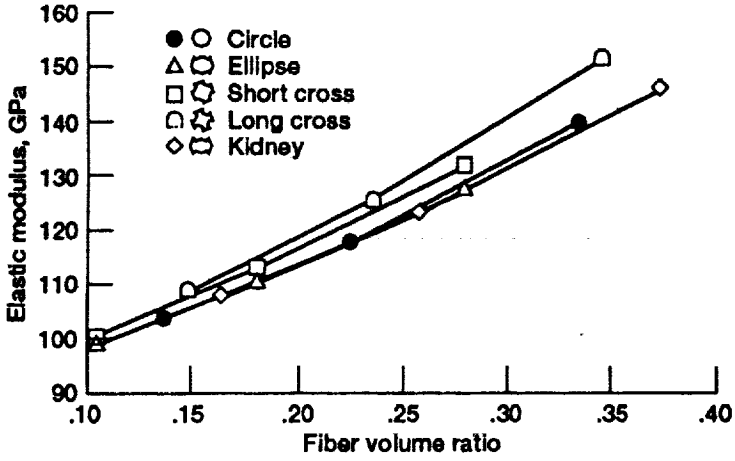

Figure A-1.—Influence of fiber shape on transverse modulus (E_{33}) of SiC/Ti-15-3.

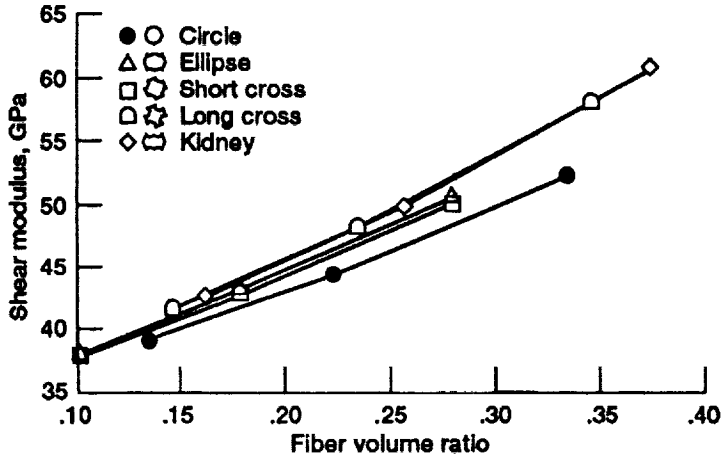

Figure A-2.—Influence of fiber shape on shear modulus (G_{21}) of SiC/Ti-15-3.

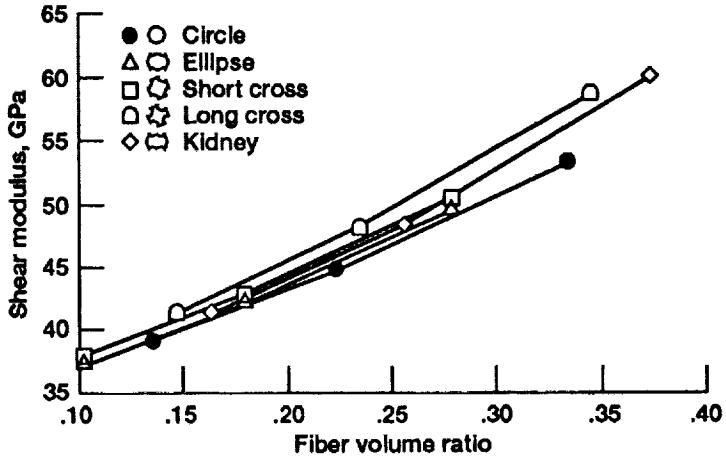

Figure A-3.—Influence of fiber shape on shear modulus (G_{23}) of SiC/Ti-15-3.

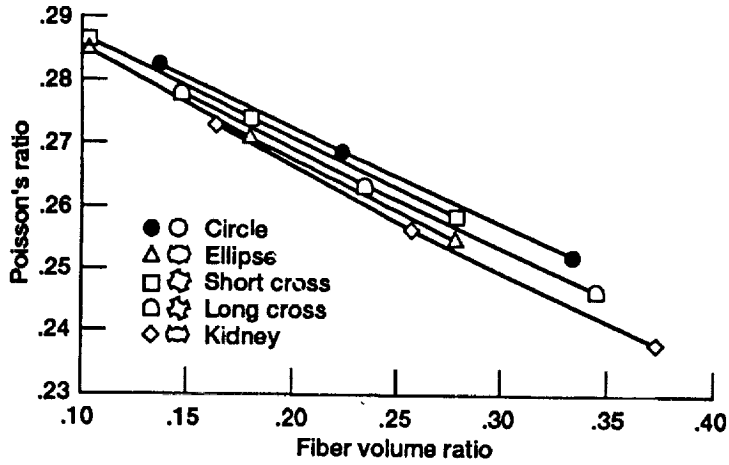

Figure A-4.—Influence of fiber shape on Poisson's ratio (ν_{12}) of SiC/Ti-15-3.

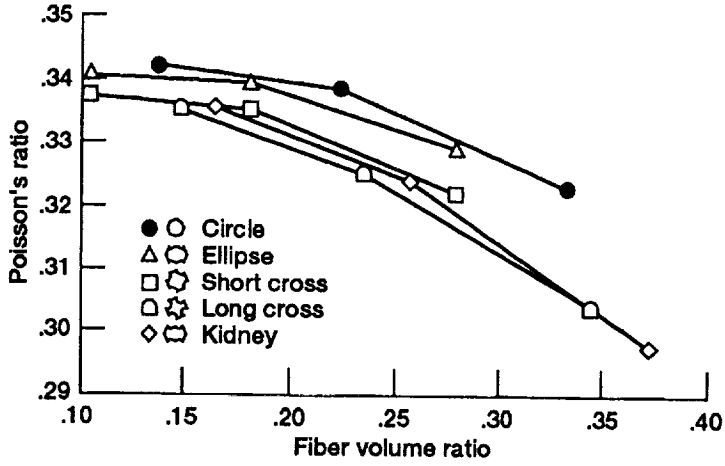

Figure A-5.—Influence of fiber shape on Poisson's ratio (ν_{23}) of SiC/Ti-15-3.

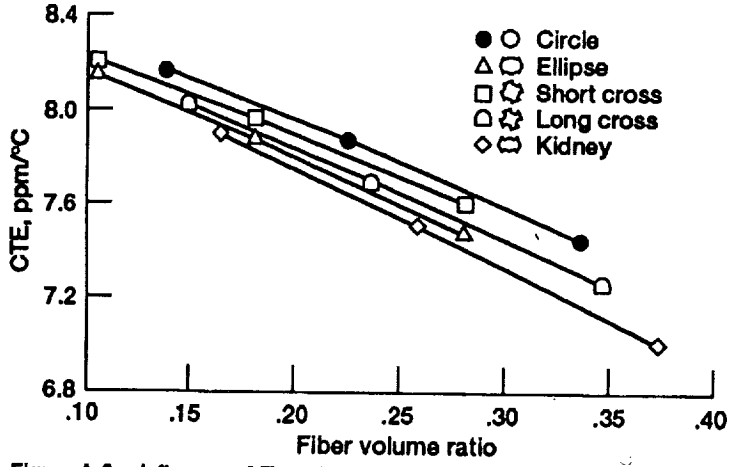

Figure A-6.—Influence of fiber shape on transverse coefficient of thermal expansion (α_{22}) of SiC/Ti-15-3.

Appendix B:

Additional Microstress Figures

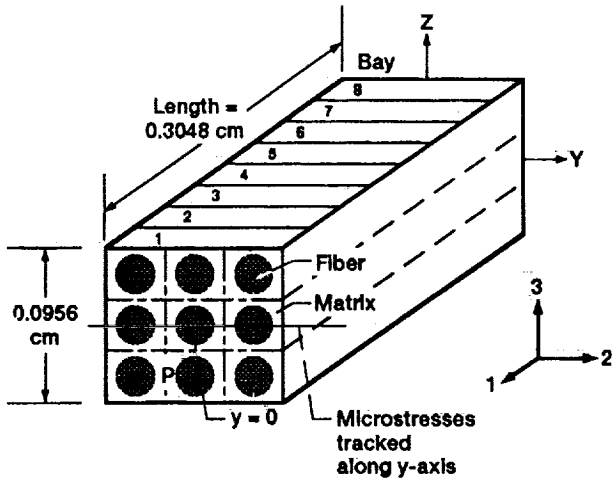

Figure B-1.—Plane where microstresses were computed.

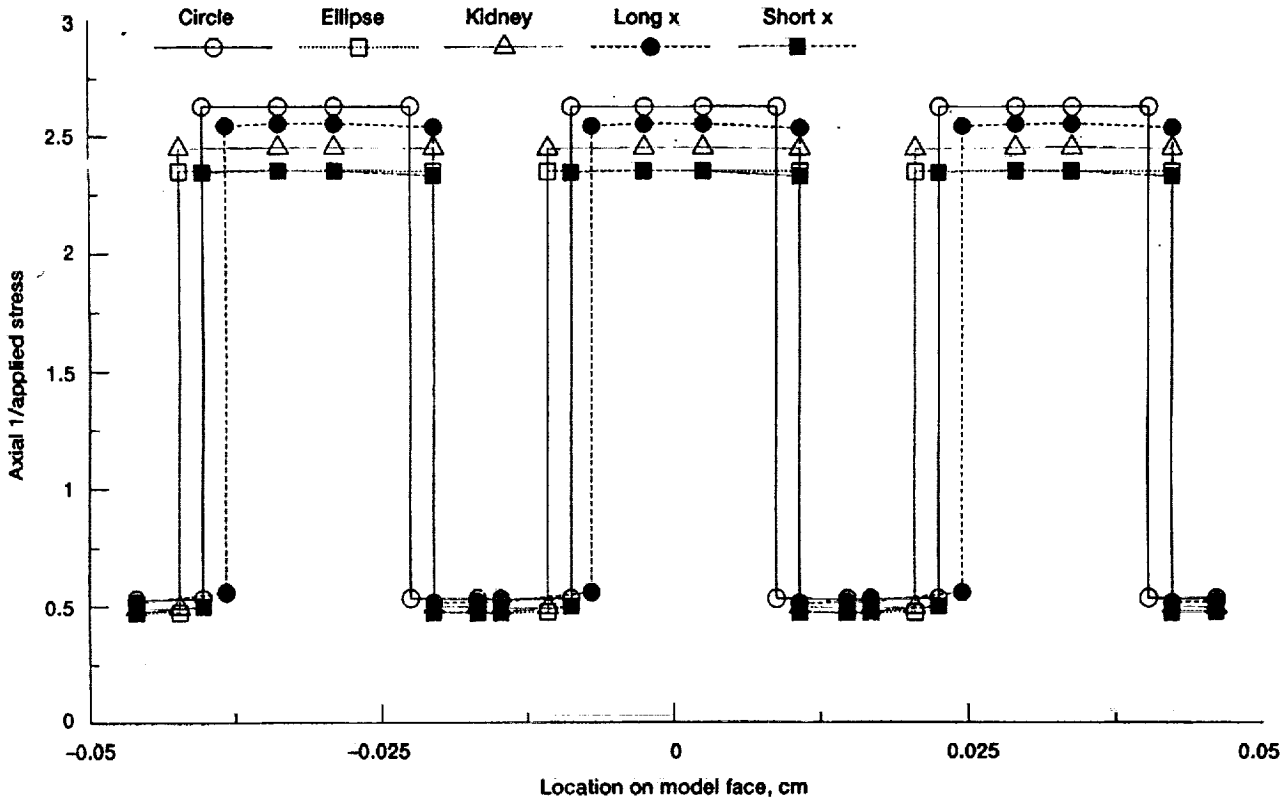

Figure B-2.—Fiber shape effects on axial microstresses under axial loading.

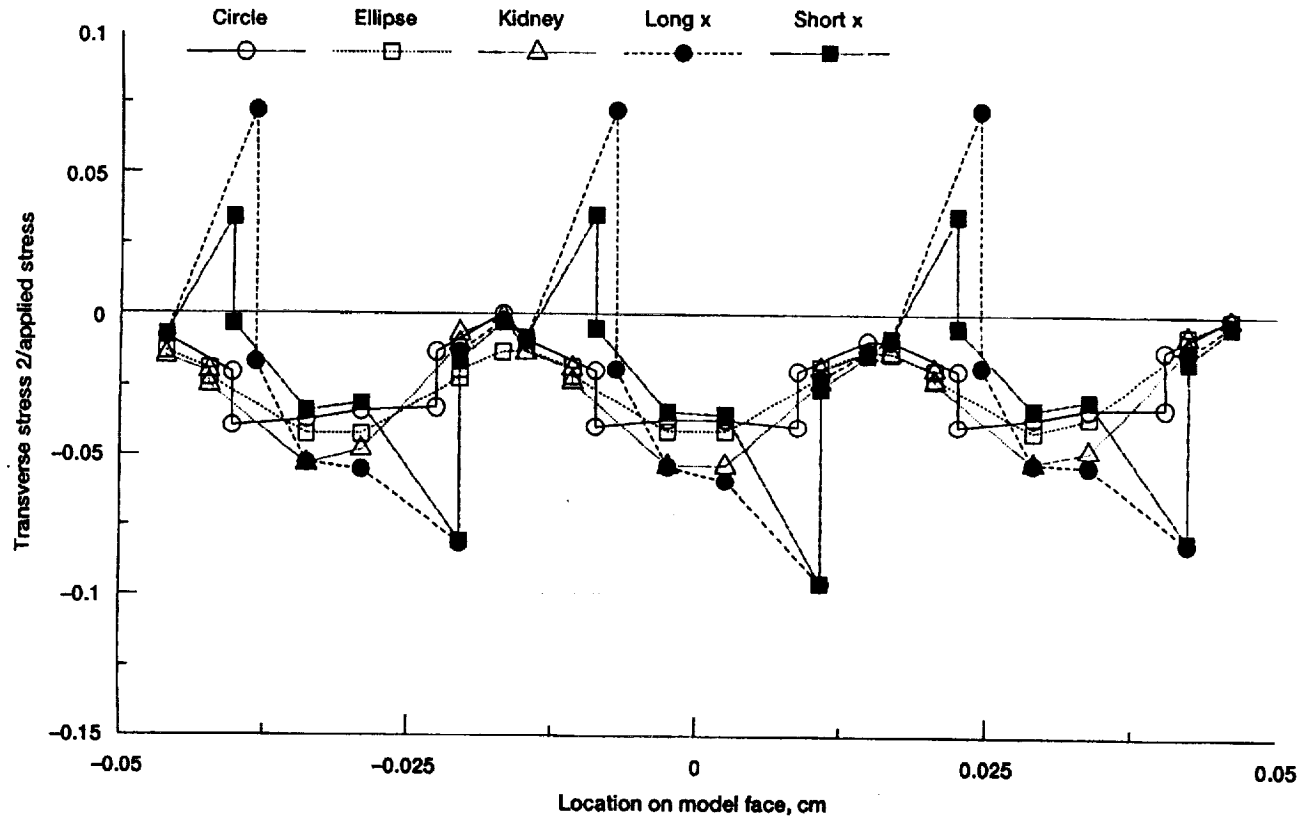

Figure B-3.—Fiber shape effects on transverse microstresses under axial loading.

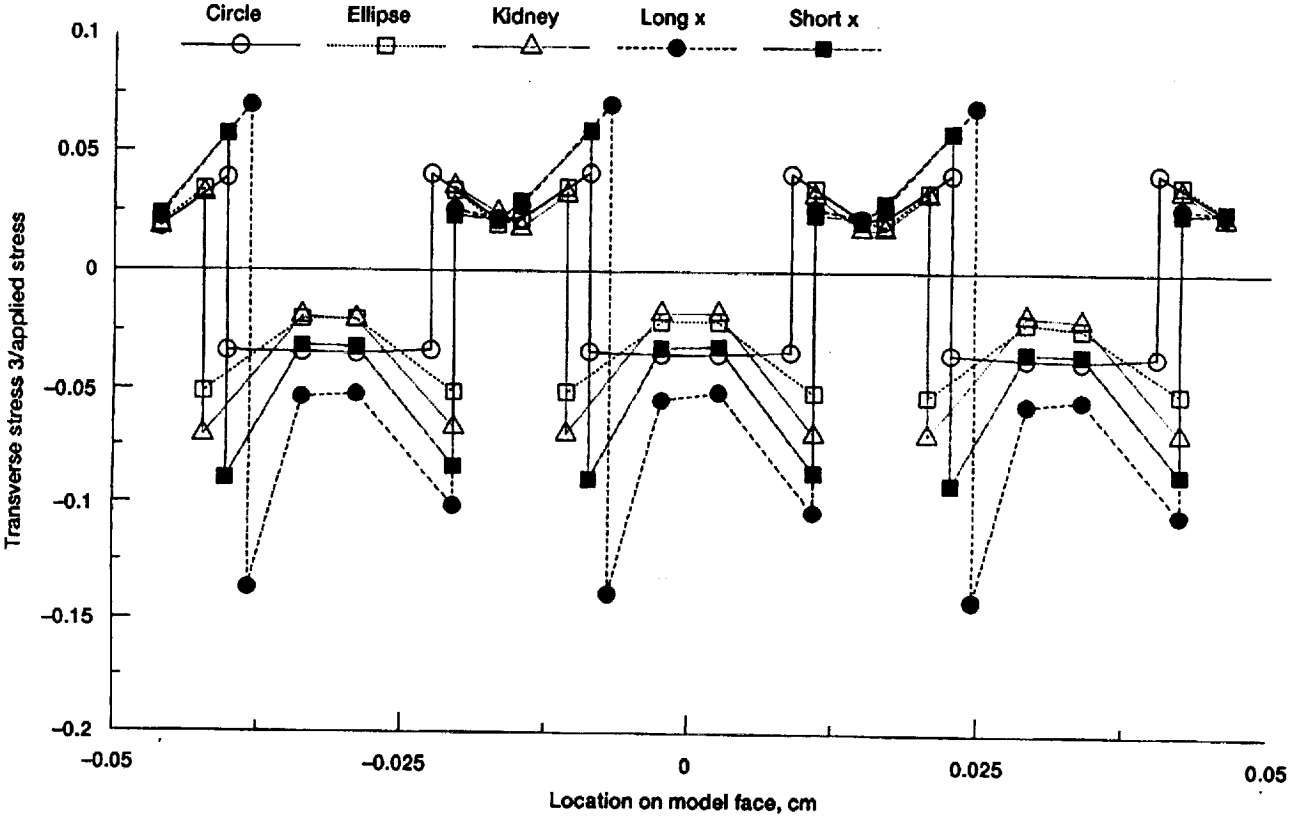

Figure B-4.—Fiber shape effects on transverse microstresses under axial loading.

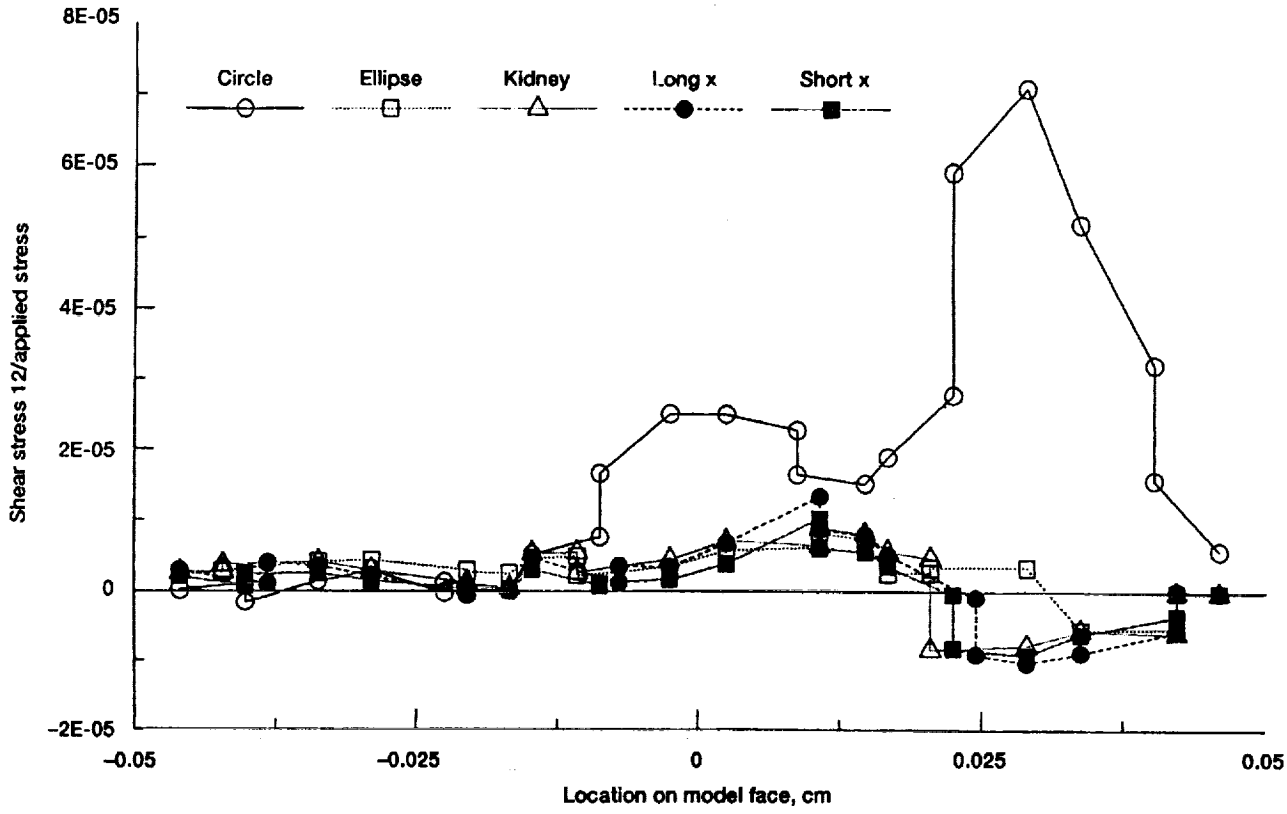

Figure B-5.—Fiber shape effects on shear microstresses under axial loading.

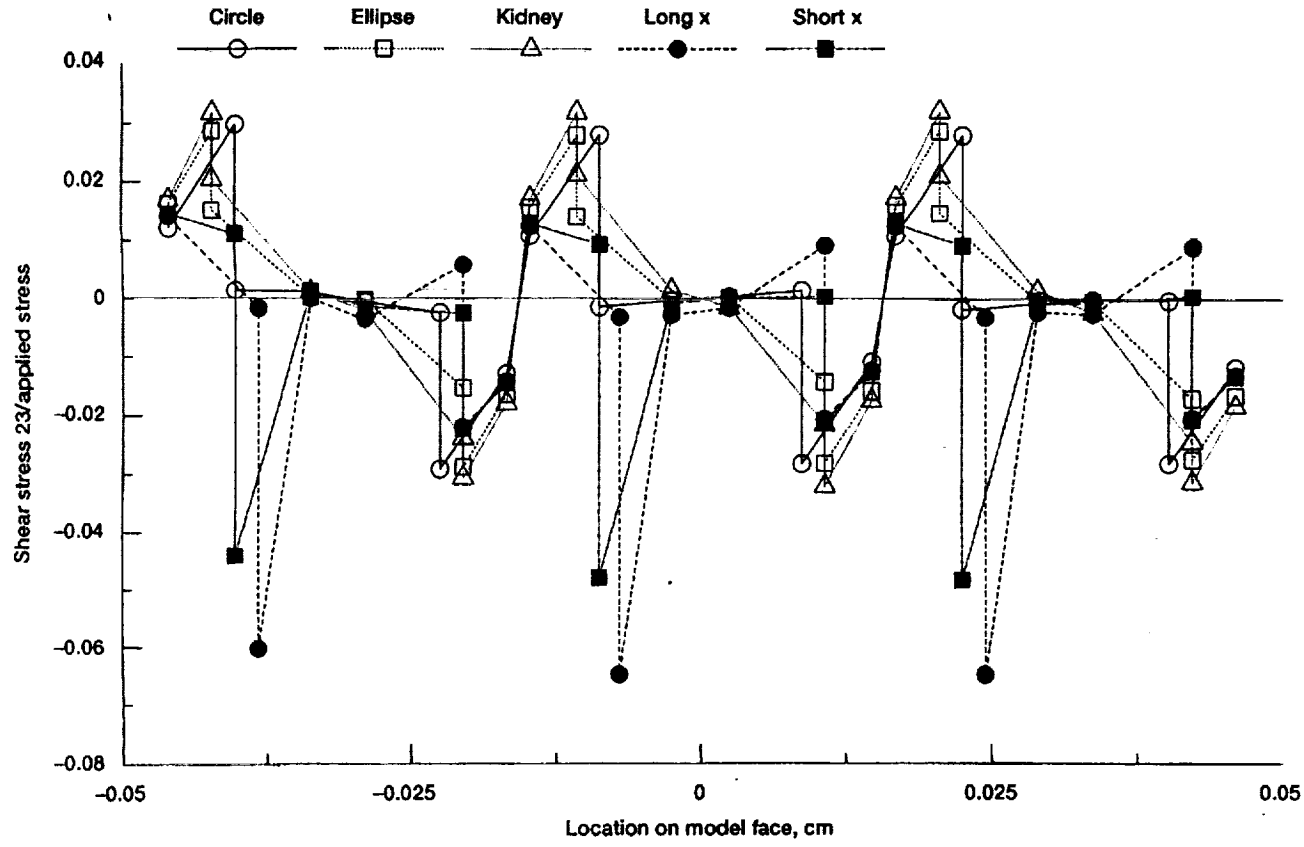

Figure B-6.—Fiber shape effects on shear microstresses under axial loading.

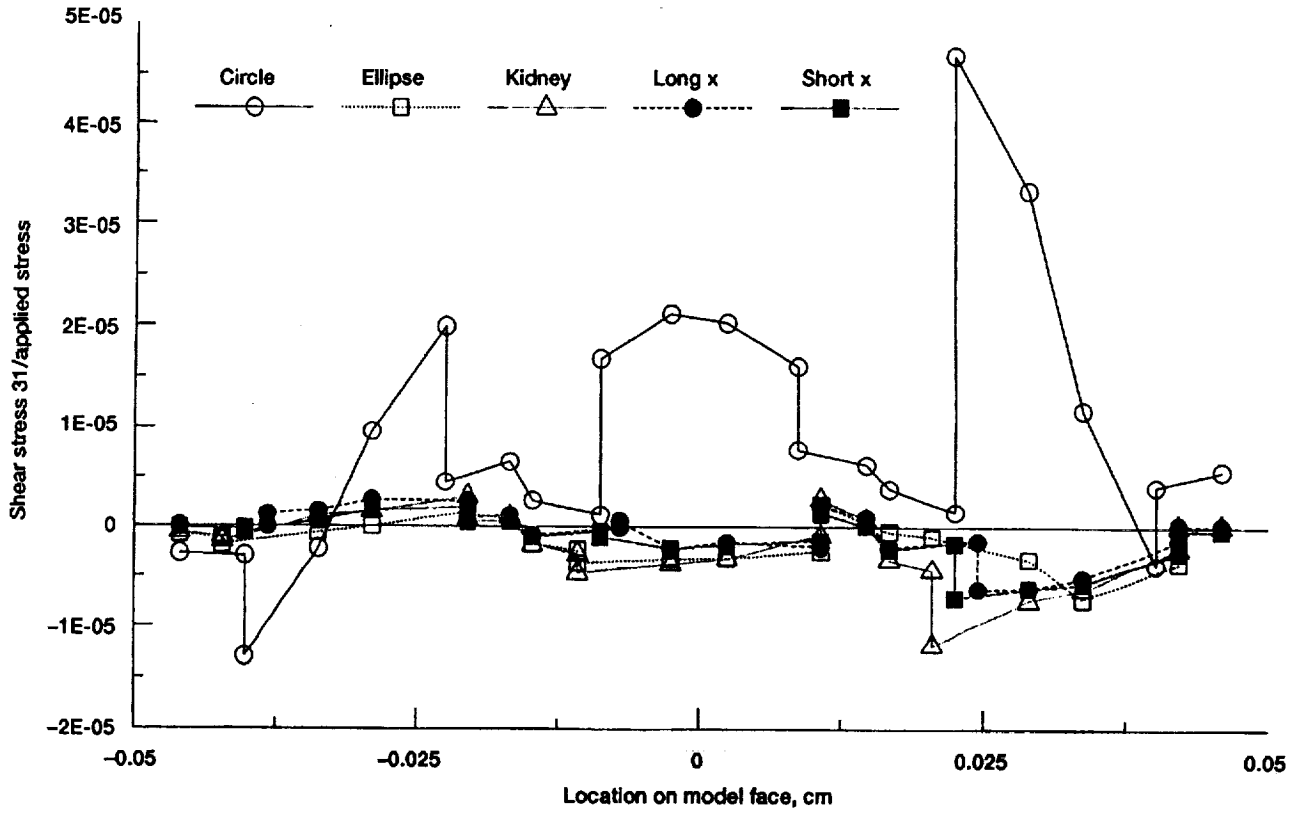

Figure B-7.—Fiber shape effects on shear microstresses under axial loading.

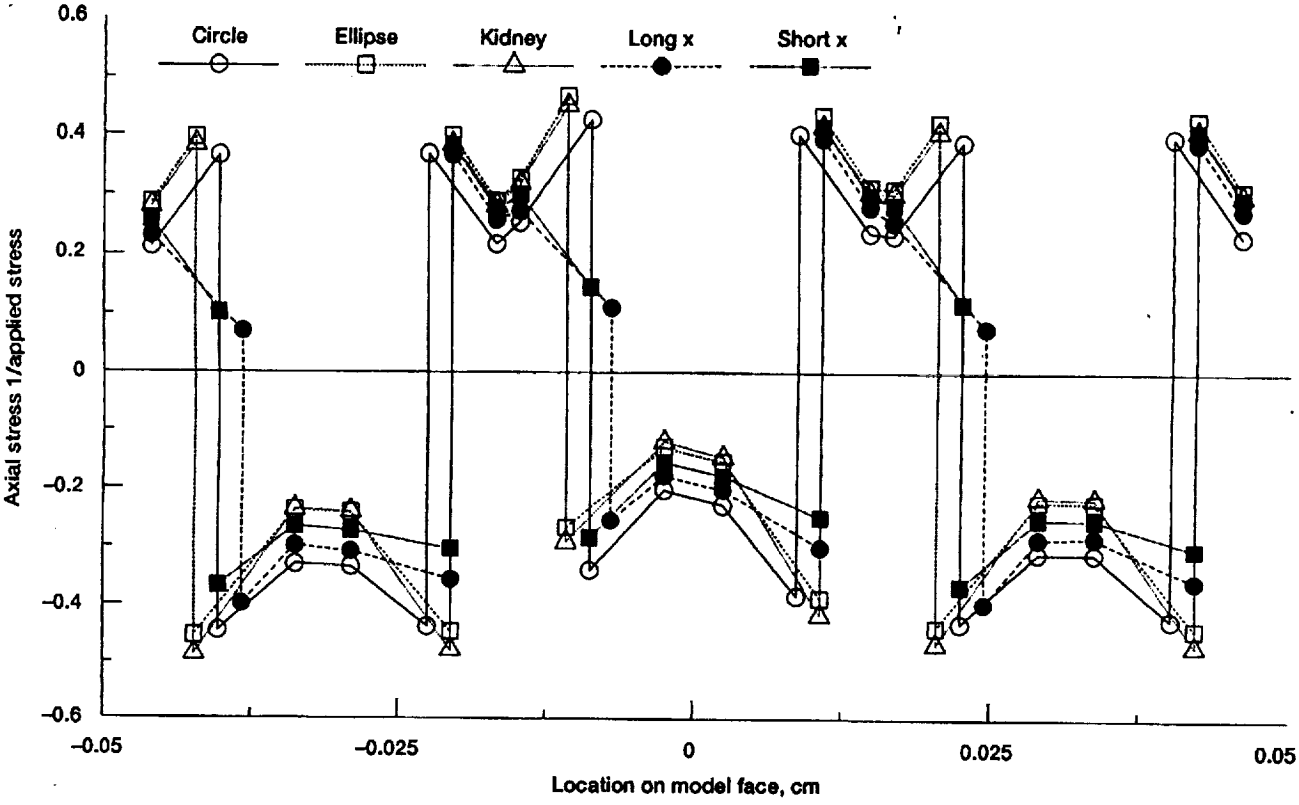

Figure B-8.—Fiber shape effects on axial microstresses under transverse loading.

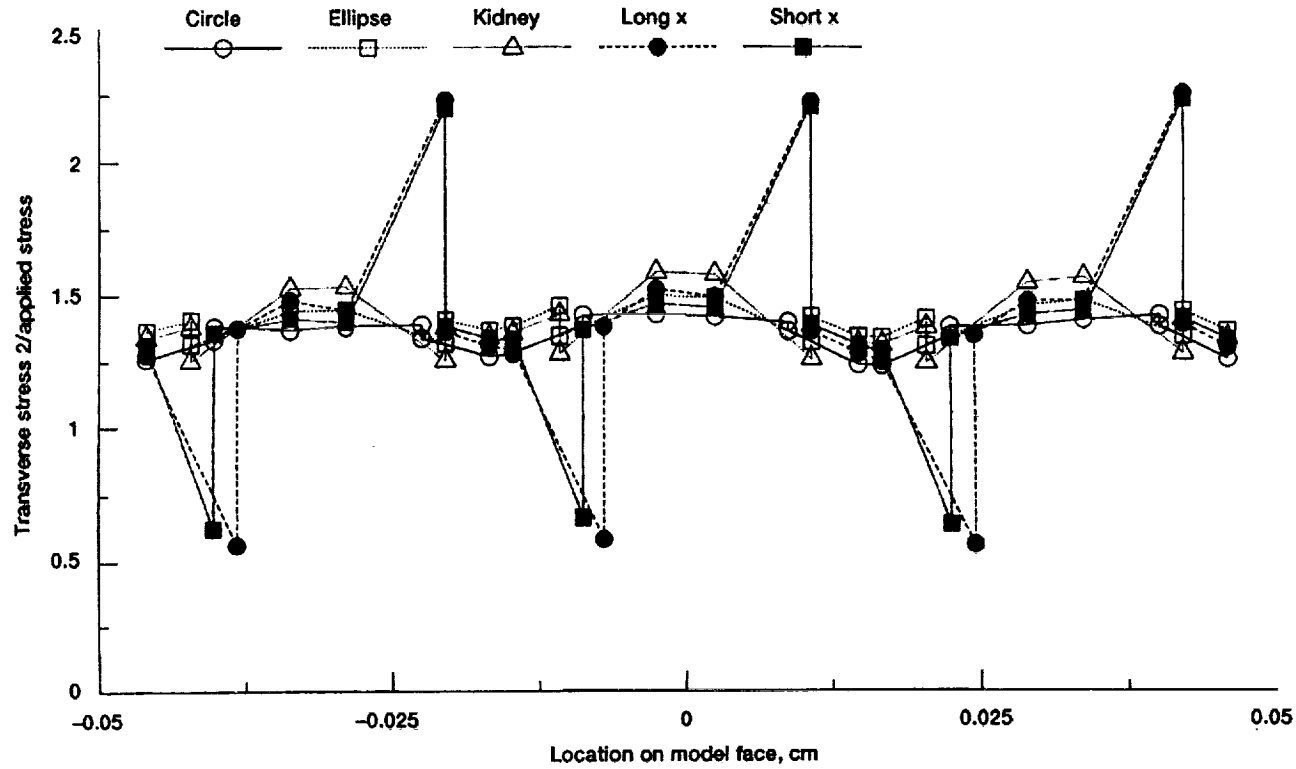

Figure B-9.—Fiber shape effects on transverse microstresses under transverse loading.

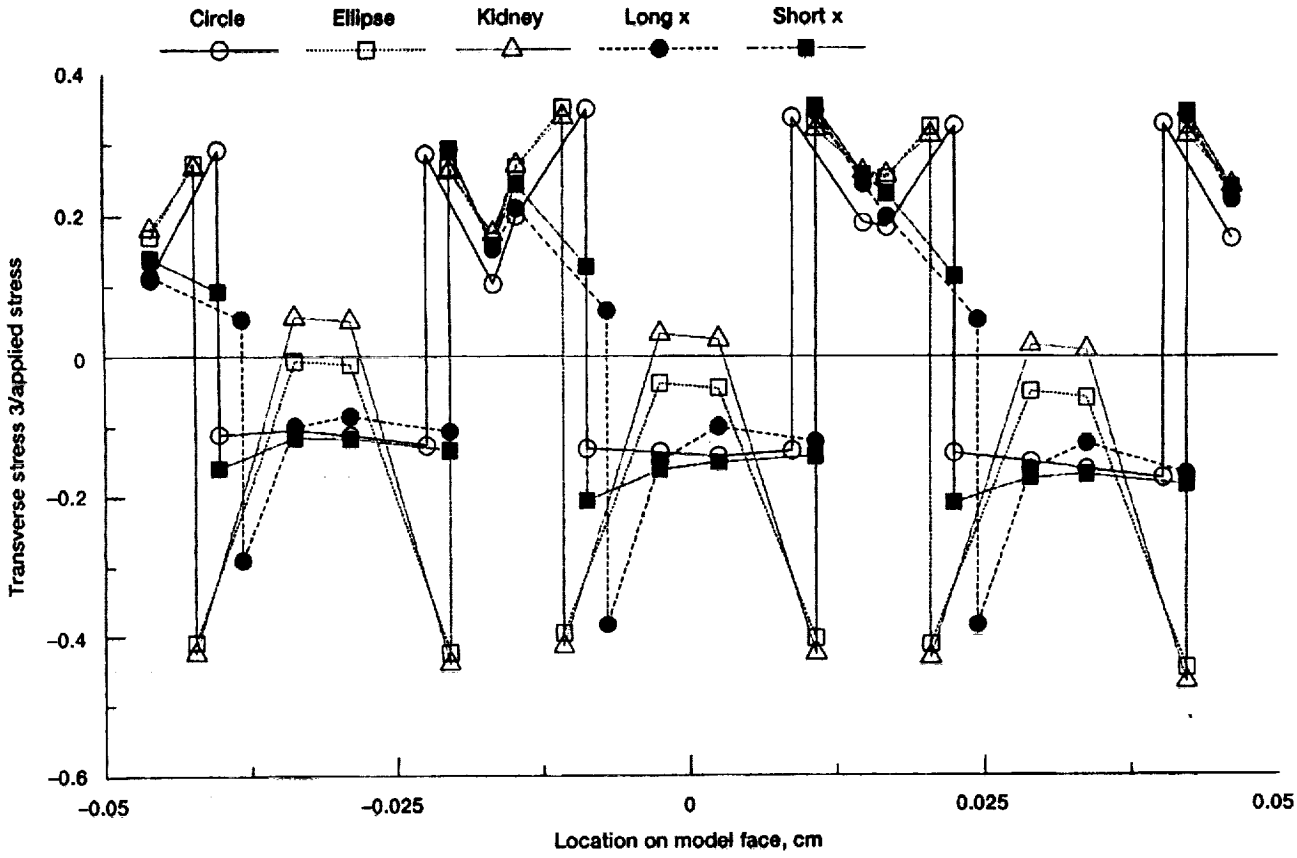

Figure B-10.—Fiber shape effects on transverse microstresses under transverse loading.

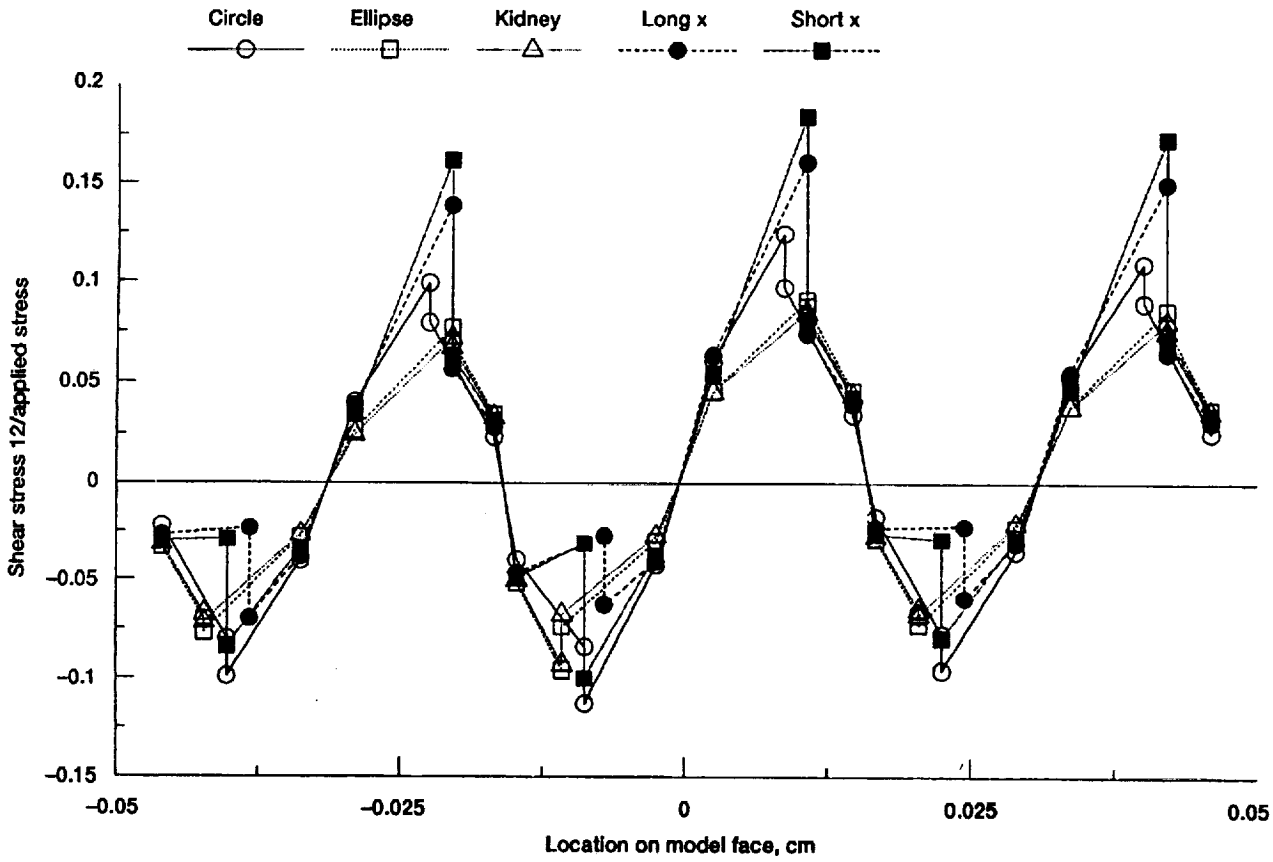

Figure B-11.—Fiber shape effects on stress microstresses under transverse loading.

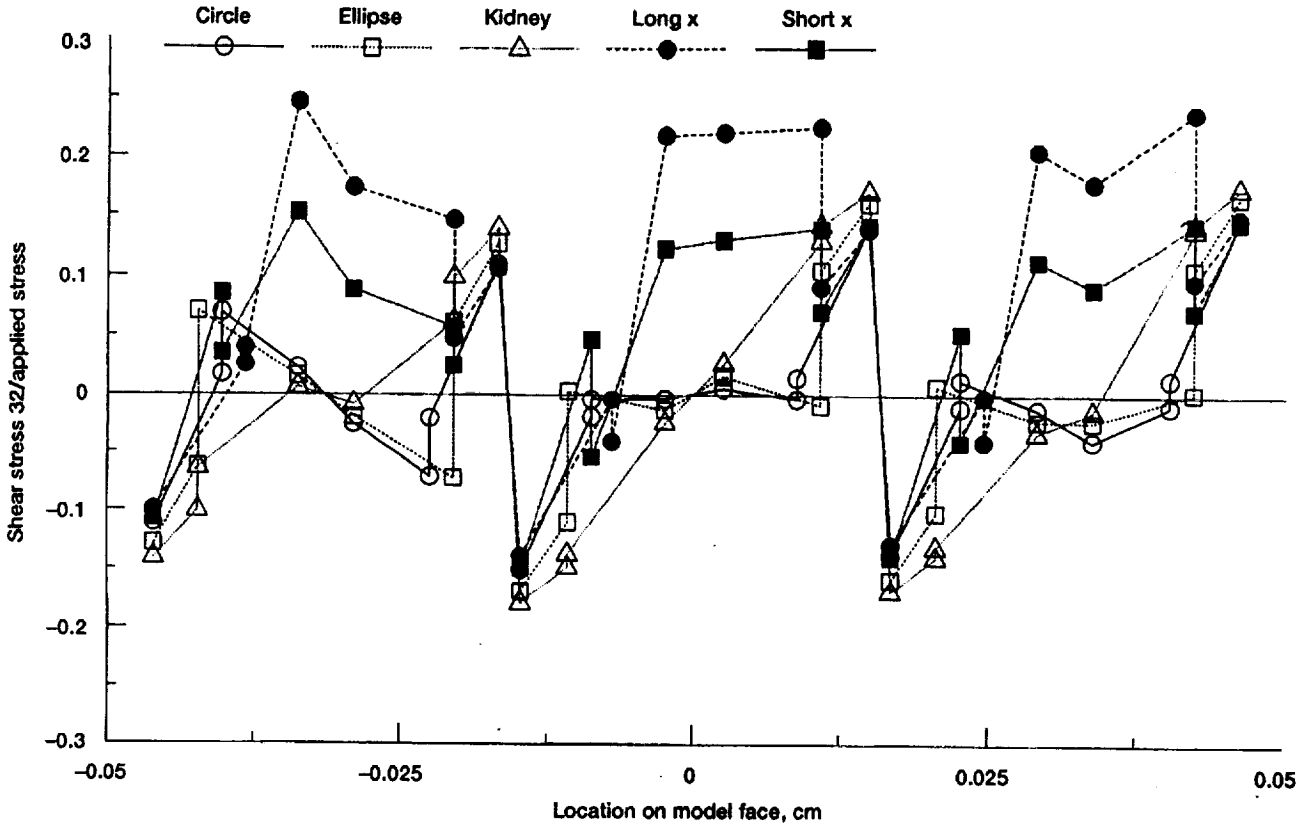

Figure B-12.—Fiber shape effects on shear microstresses under transverse loading.

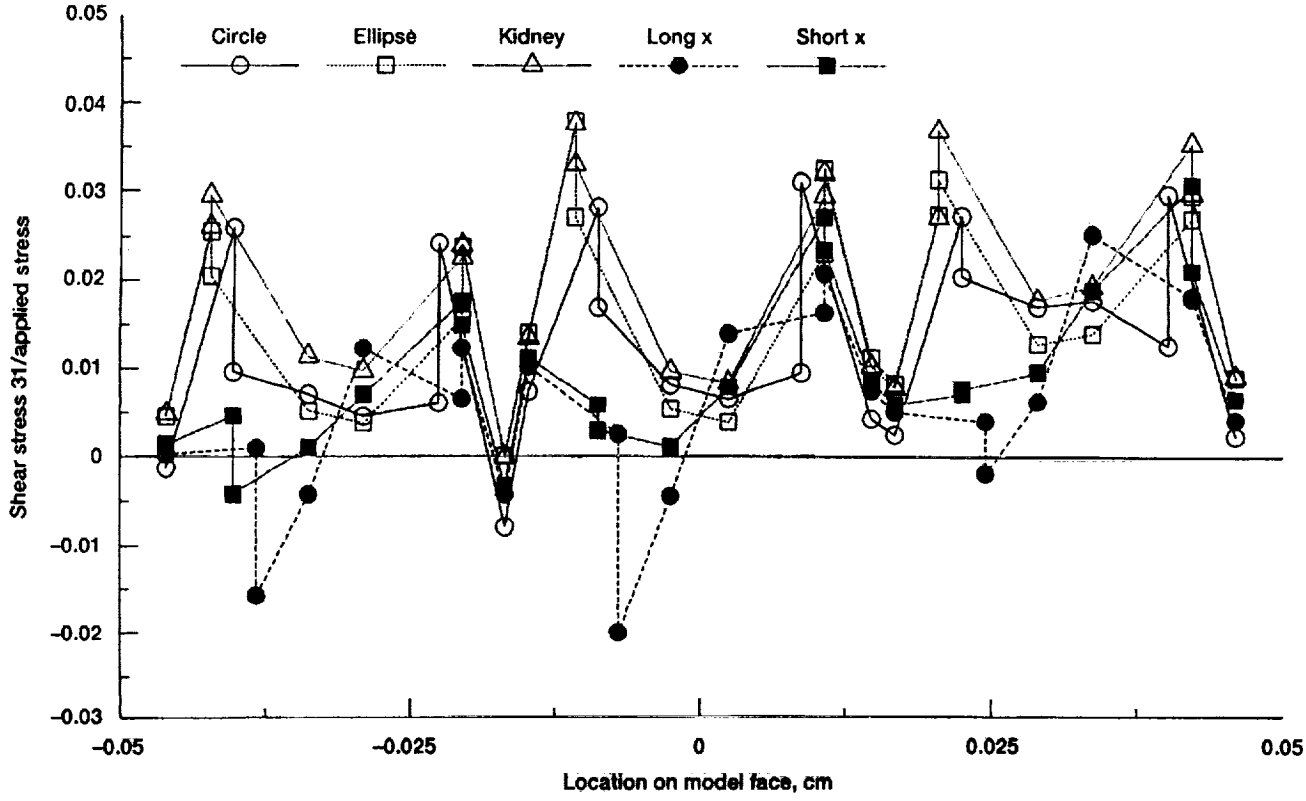

Figure B-13.—Fiber shape effects on shear microstresses under transverse loading.

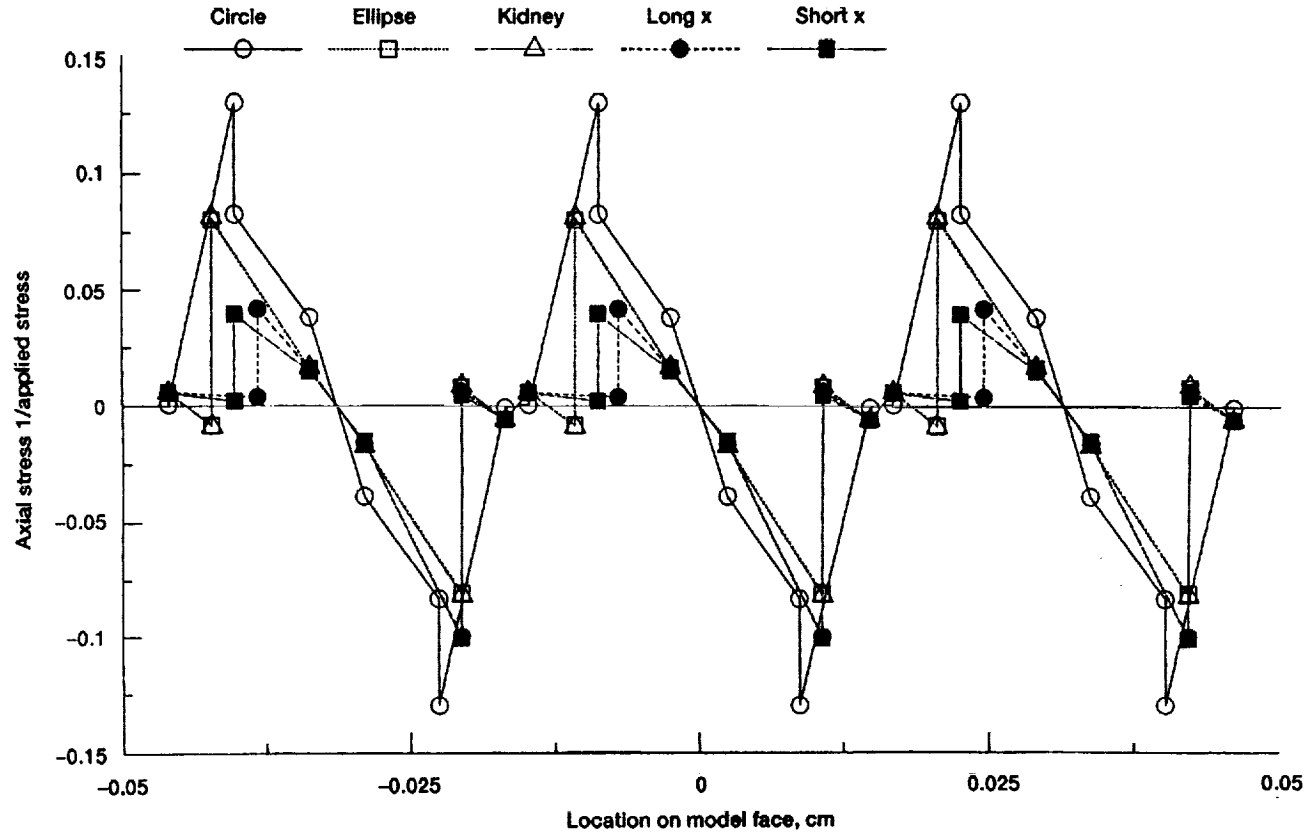

Figure B-14.—Fiber shape effects on axial microstresses under shear loading.

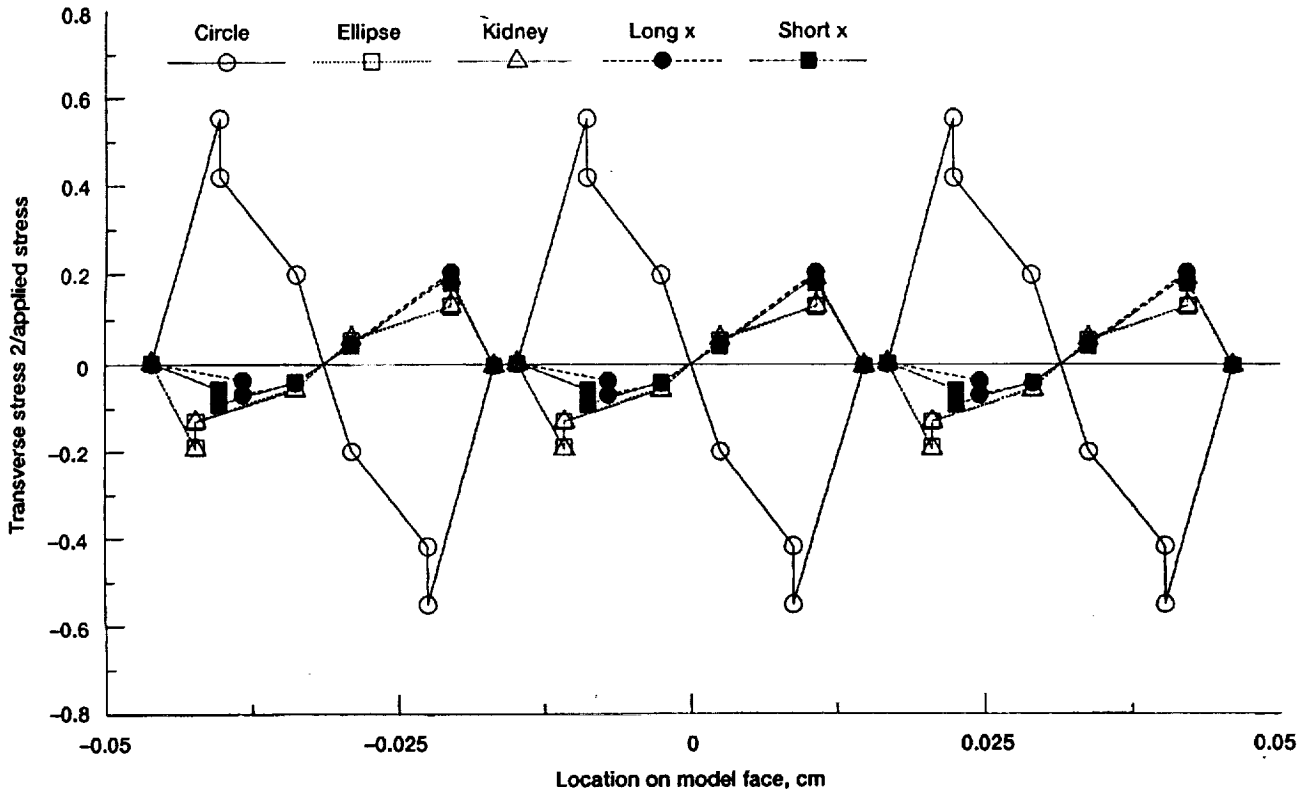

Figure B-15.—Fiber shape effects on transverse microstresses under shear loading.

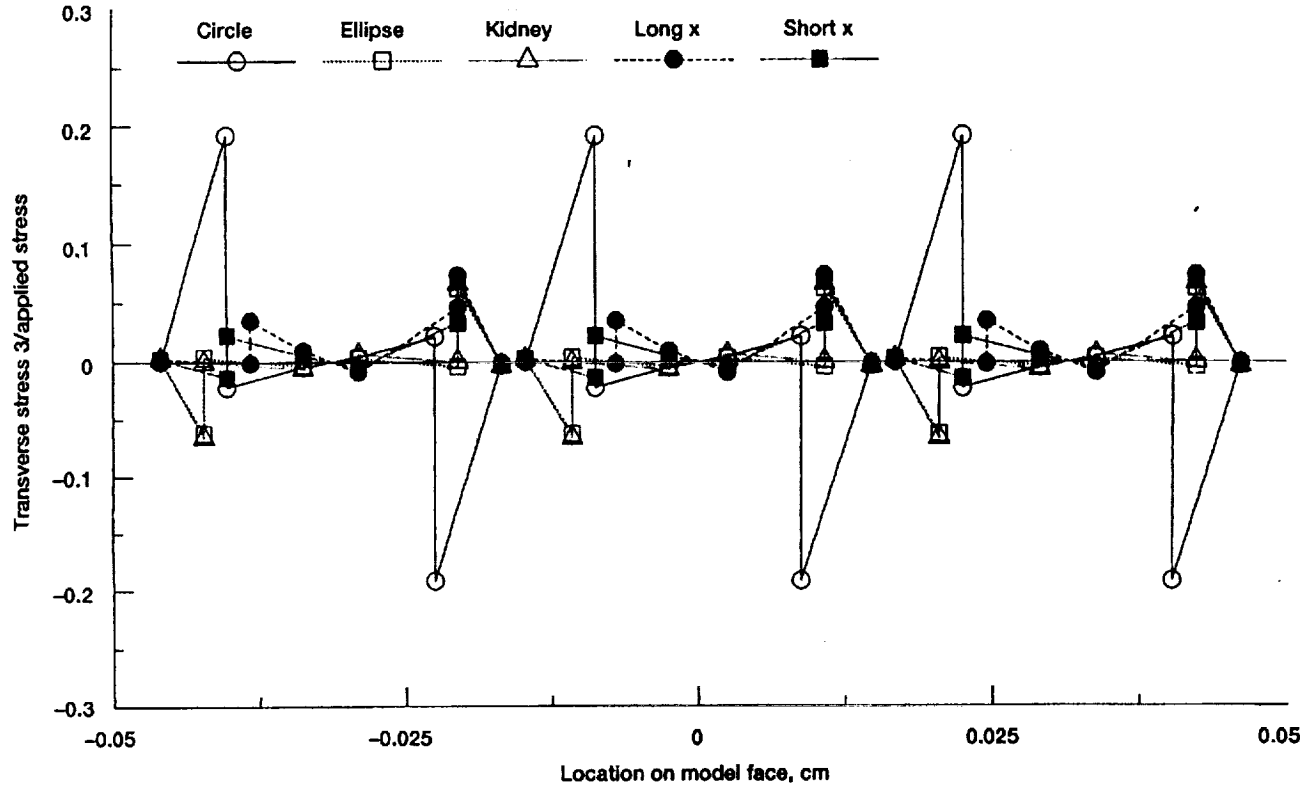

Figure B-16.—Fiber shape effects on transverse microstresses under shear loading.

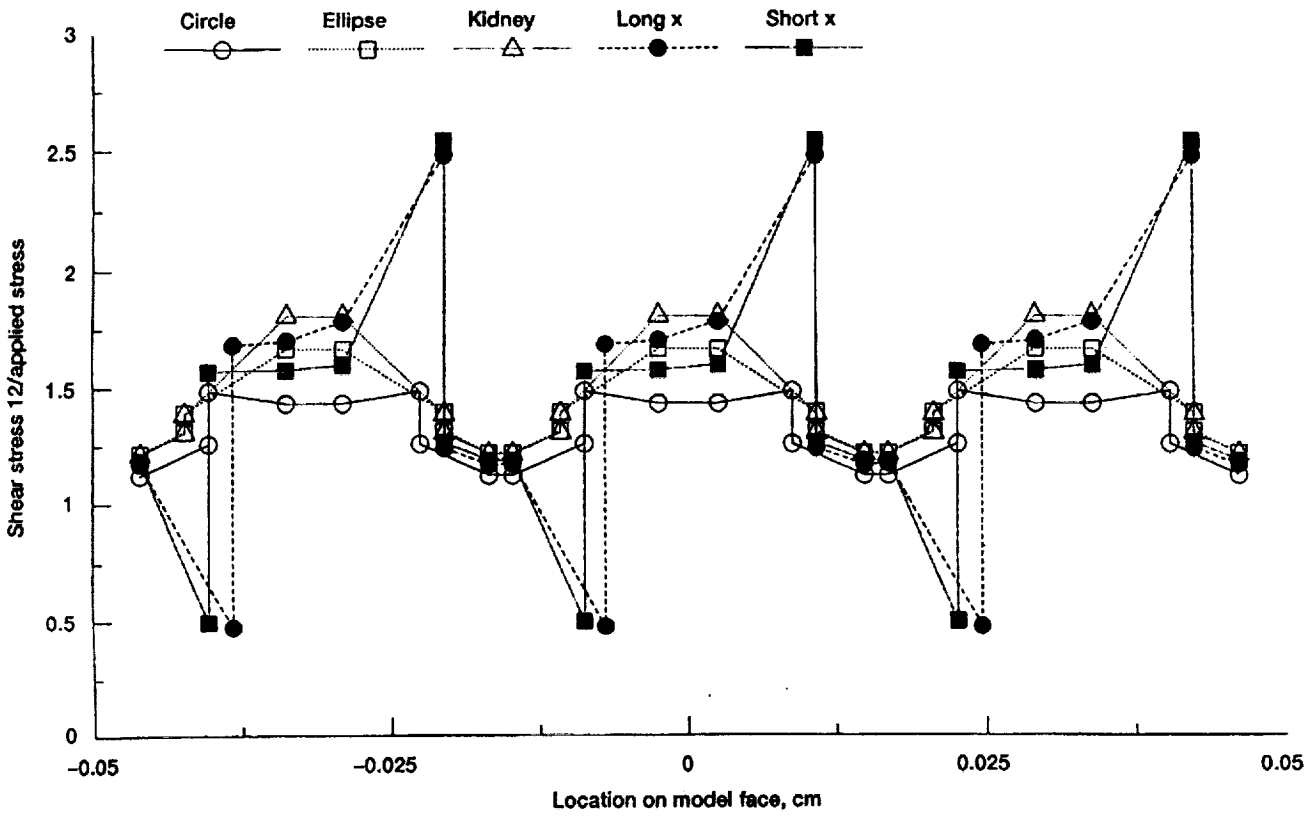

Figure B-17.—Fiber shape effects on shear microstresses under shear loading.

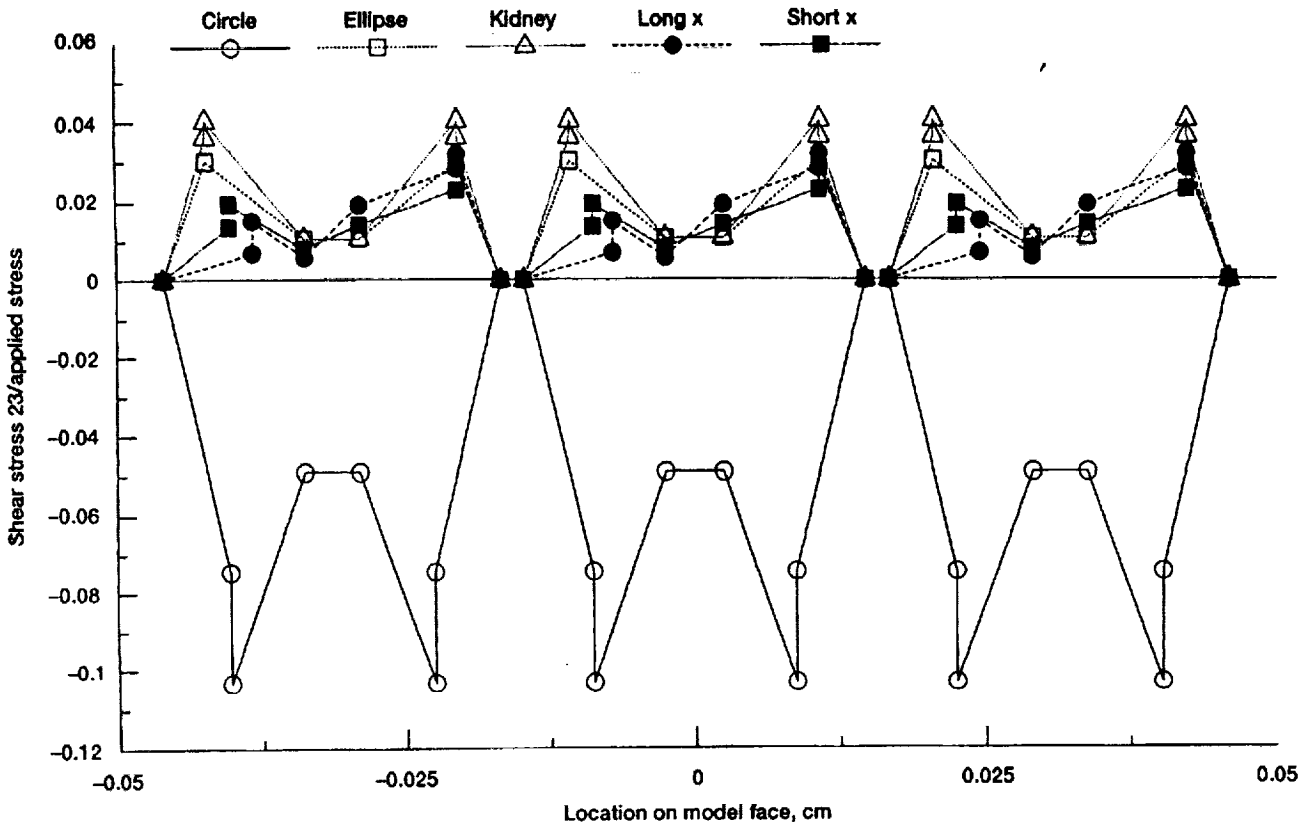

Figure B-18.—Fiber shape effects on shear microstresses under shear loading.

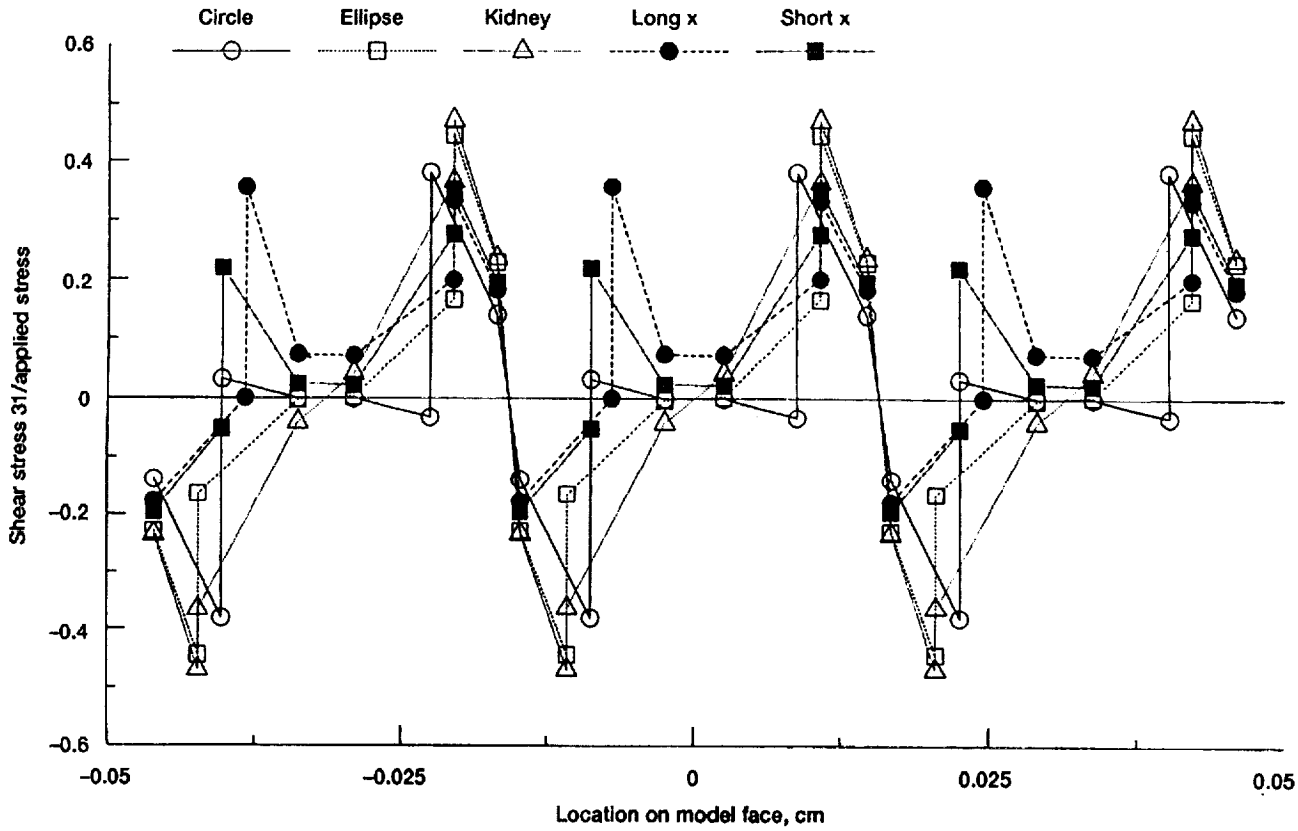

Figure B-19.—Fiber shape effects on shear microstresses under shear loading.

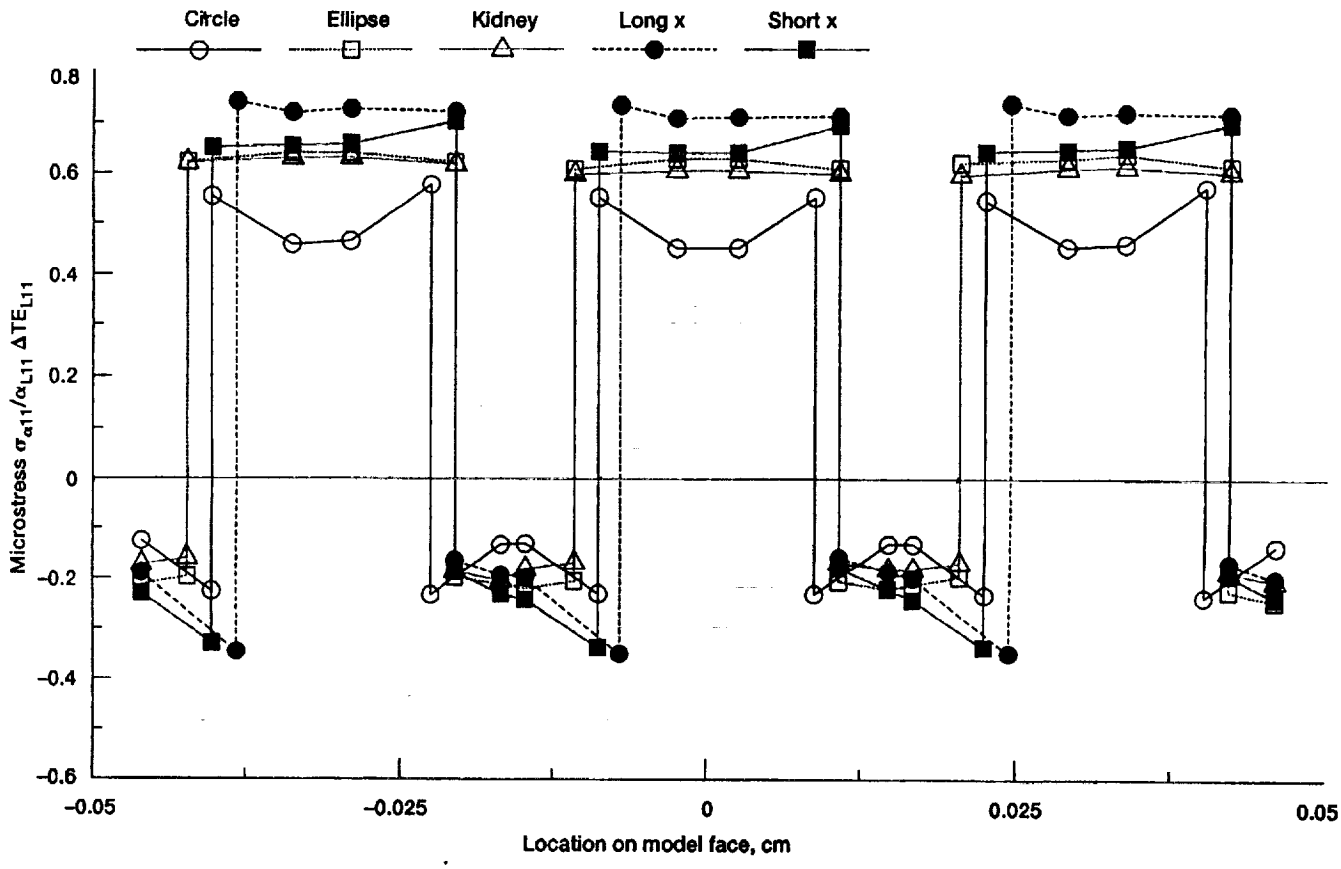

Figure B-20.—Fiber shape effects on axial microstresses under thermal loading.

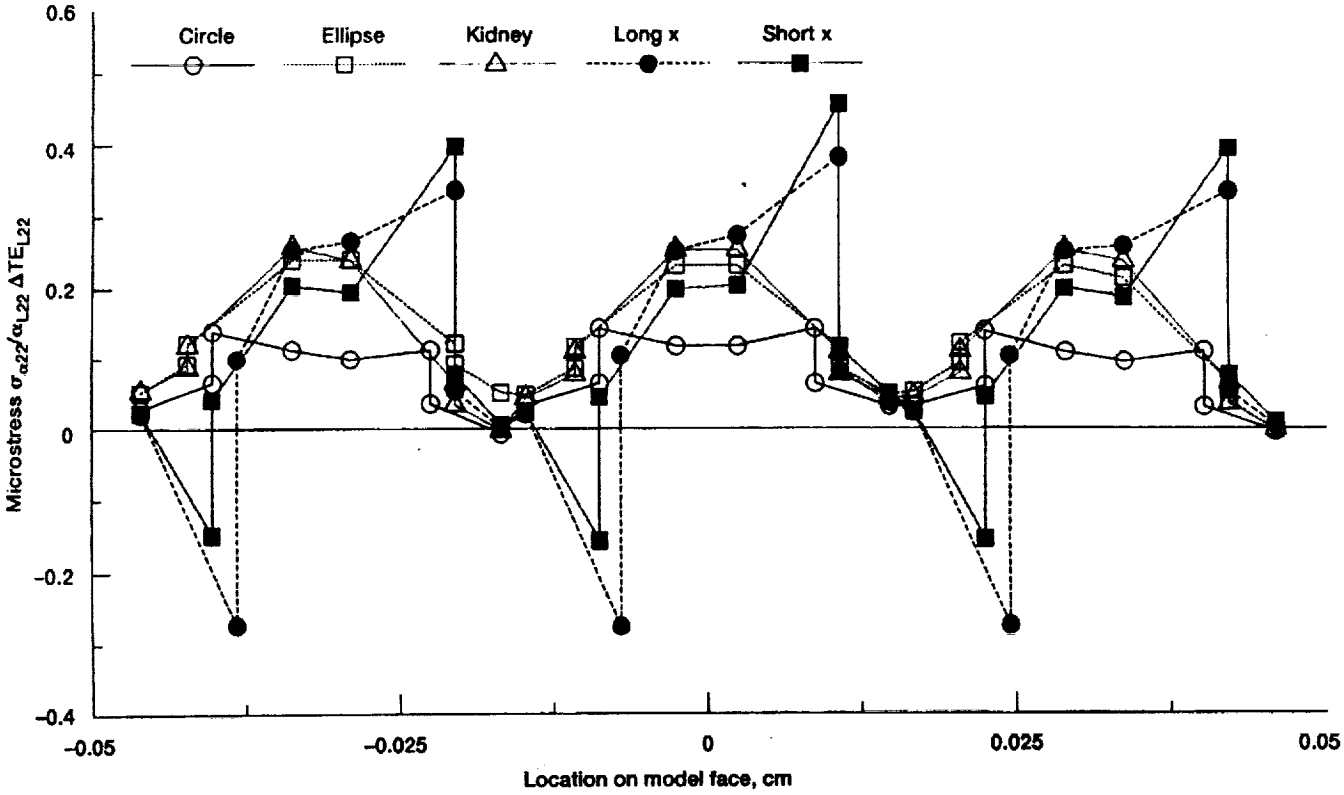

Figure B-21.—Fiber shape effects on transverse microstresses under thermal loading.

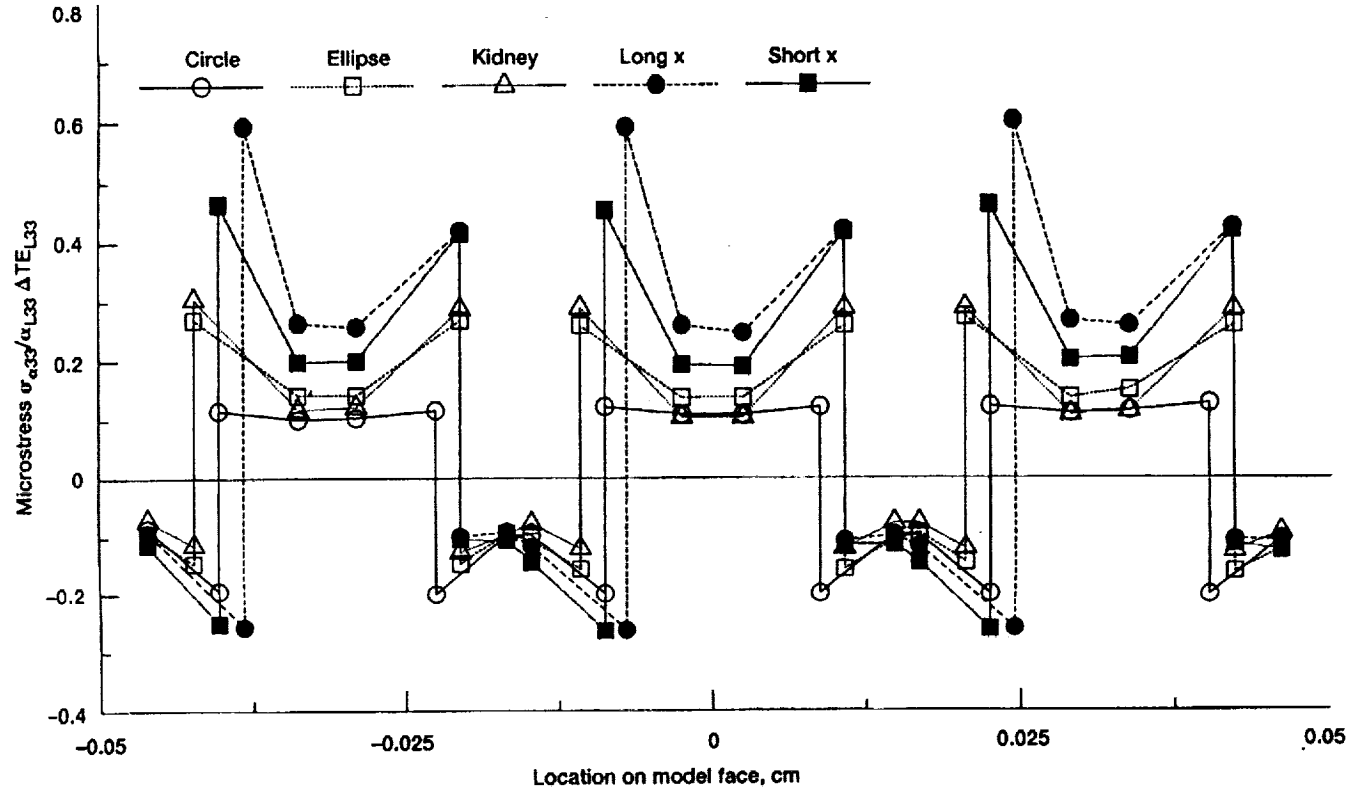

Figure B-22.—Fiber shape effects on transverse microstresses under thermal loading.

REPORT DOCUMENTATION PAGE

Form Approved
OMB No. 0704-0188

1. AGENCY USE ONLY (*Leave blank*)	2. REPORT DATE	3. REPORT TYPE AND DATES COVERED
	March 1992	Technical Memorandum

4. TITLE AND SUBTITLE

Fiber Shape Effects on Metal Matrix Composite Behavior

5. FUNDING NUMBERS

WU–510–01–50

6. AUTHOR(S)

H.C. Brown, H.-J. Lee, and C.C. Chamis

7. PERFORMING ORGANIZATION NAME(S) AND ADDRESS(ES)

National Aeronautics and Space Administration
Lewis Research Center
Cleveland, Ohio 44135–3191

8. PERFORMING ORGANIZATION REPORT NUMBER

E–7672

9. SPONSORING/MONITORING AGENCY NAMES(S) AND ADDRESS(ES)

National Aeronautics and Space Administration
Washington, D.C. 20546–0001

10. SPONSORING/MONITORING AGENCY REPORT NUMBER

NASA TM–106067

11. SUPPLEMENTARY NOTES

Prepared for the 37th International SAMPE Symposium and Exhibition sponsored by the Society for the Advancement of Materials and Process Engineering, Anaheim, California, March 9–12, 1992. H.C. Brown, Sverdrup Technology, Inc., Lewis Research Center Group, 2001 Aerospace Parkway, Brook Park, Ohio 44142. H.-J. Lee and C.C. Chamis, NASA Lewis Research Center. Responsible person, H.-J. Lee (216) 433–3316.

12a. DISTRIBUTION/AVAILABILITY STATEMENT

Unclassified - Unlimited
Subject Category 24

12b. DISTRIBUTION CODE

13. ABSTRACT ***(Maximum 200 words)***

The effects of different fiber shapes on the behavior of a SiC/Ti-15 metal matrix composite is computationally simulated. A three-dimensional finite element model consisting of a group of nine unidirectional fibers is used in the analysis. The model is employed to represent five different fiber shapes: a circle, an ellipse, a kidney, and two different cross shapes. The distribution of microstresses and the composite material properties, such as moduli, coefficients of thermal expansion, and Poisson's ratios, are obtained from the finite element analysis for the various fiber shapes. Comparisons of these results are used to determine the sensitivity of the composite behavior to the different fiber shapes and assess their potential benefits. No clear benefits result from different fiber shapes though there are some increases/decreases in isolated properties.

14. SUBJECT TERMS

Composite properties; Fiber shapes; Finite element analysis; Material properties; Metal matrix composite; Microstresses

15. NUMBER OF PAGES
34

16. PRICE CODE
A03

17. SECURITY CLASSIFICATION OF REPORT	18. SECURITY CLASSIFICATION OF THIS PAGE	19. SECURITY CLASSIFICATION OF ABSTRACT	20. LIMITATION OF ABSTRACT
Unclassified	Unclassified	Unclassified	